A&A 517, A24 (2010)
DOI: 10.1051/0004-6361/201014477

Astronomy & Astrophysics

Properties and nature of Be stars⋆,⋆⋆

28. Implications of systematic observations for the nature of the multiple system with the Be star *o* Cassiopeæ and its circumstellar environment

P. Koubský[1], C. A. Hummel[2], P. Harmanec[3], C. Tycner[4], F. van Leeuwen[5], S. Yang[6], M. Šlechta[1], H. Božić[7], R. T. Zavala[8], D. Ruždjak[7], and D. Sudar[7]

[1] Astronomical Institute, Academy of Sciences of the Czech Republic, 251 65 Ondřejov, Czech Republic
e-mail: koubsky@sunstel.asu.cas.cz
[2] European Organisation for Astronomical Research in the Southern Hemisphere, Karl-Schwarzschild-Str. 2, 85748 Garching bei München, Germany
[3] Astronomical Institute of the Charles University, Faculty of Mathematics and Physics, V Holešovičkách 2, 180 00 Praha 8 - Troja, Czech Republic
[4] Department of Physics, Central Michigan University, Mount Pleasant, MI 48859, USA
[5] Institute of Astronomy, Madingley Road, Cambridge, UK
[6] University of Victoria, Dept of Physics and Astronomy, PO Box 3055 Victoria, BC V8W 3P6, Canada
[7] Hvar Observatory, Faculty of Geodesy, Zagreb University, Kačiceva 26, 10000 Zagreb, Croatia
[8] US Naval Observatory, Flagstaff Station, 10391 West Naval Observatory Road, Flagstaff, AZ 86001, USA

Received 22 March 2010 / Accepted 19 April 2010

ABSTRACT

The analysis of radial velocities of the Be star *o* Cas from spectra taken between 1992 and 2008 at the Ondřejov Observatory and the Dominion Astrophysical Observatory allowed us to reconfirm the binary nature of this object, first suggested by Abt and Levy in 1978, but later refuted by several authors. The orbital parameters of this SB1 system imply a very high mass function of about one solar mass. This in turn leads to a very high mass of the secondary, possibly higher than that of the primary. In order to look for such a massive secondary, *o* Cas was observed with the Navy Prototype Optical Interferometer, which allowed the binary components to be spatially resolved for the first time. The interferometric observations lead to the detection of a secondary, about 3 mag fainter than the primary. The possible properties of this peculiar binary system and the reasons why the massive secondary does not dominate the optical spectrum are discussed.

Key words. binaries: close – binaries: spectroscopic – stars: emission-line, Be – stars: fundamental parameters – stars: individual: *o* Cas

1. Introduction

o Cas (HD 4180, HR 193, BD+47°183, HIP 3504) is a bright Be star ($V = 4^{m}.3$–$4^{m}.6$ var., B5III-IVe, $v \sin i = 220$ km s^{-1}). It is also the brighter component of the wide double system WDS 00447+4817 (Mason, Wycoff & Hartkopf, http://ad.usno.navy.mil/wds). This system exhibits little or no orbital motion over the time interval of available observations (separation 32.″8–33.″8), and the fainter component is an 11-mag. star. Spectral variability of *o* Cas was reported by several authors. A good summary of the historical records of Hα profile changes can be found in Peton (1972). The Hα emission apparently persisted from the early 1930's to the early 1950's. Hubert-Delplace & Hubert (1979) stated that *o* Cas was without emission from 1953 to 1959. Between December 1975 and November 1976, another emission episode started and continued through the early 1980's (Slettebak & Reynolds 1978; Andrillat & Fehrenbach 1982). In December 1982 the Hα emission reached an intensity of 2.0 relative to the continuum (Barker 1983). The Ondřejov spectra, taken since 1992, have shown relatively strong emission in Hα (4.0 to 6.5 times the continuum intensity). This is in accordance with Christian Buil's *The spectroscopic Be-stars Atlas*[1]. Photometric variability of *o* Cas was first reported by Haupt & Schroll (1974). Pavlovski et al. (1997) summarized the observations of *o* Cas at Hvar from about HJD 2 445 000 to 2 447 900. Hubert & Floquet (1998) investigated variability of bright Be stars using *Hipparcos* photometry. For *o* Cas they detected a long-term monotonic decline of $0^{m}.06$ between HJD 2 447 800 and 2 449 200. When this trend was subtracted, a short-term variability with a period of $1^{d}.257$ and semi-amplitude $0^{m}.01$ was clearly visible.

Analyzing He I absorption radial velocities (RVs hereafter) from 20 photographic spectra, Abt & Levy (1978) (AL) proposed that *o* Cas is a single-line spectroscopic binary with an orbital period of 1033 days and an insignificant eccentricity ($e = 0.11 \pm 0.15$). Their finding was confirmed by

⋆ Based on new spectroscopic, photometric and interferometric observations from the following observatories: Dominion Astrophysical Observatory, Herzberg Institute of Astrophysics, National Research Council of Canada, Hvar, Navy Prototype Optical Interferometer, and Astronomical Institute AS CR Ondřejov.

⋆⋆ Appendices are only available in electronic form at http://www.aanda.org

[1] All his reduced individual Hα observations are made publicly available via http://www.astrosurf.com/buil

Elias et al. (1978). However, Horn et al. (1985) re-analyzed AL's RVs together with a series of high-dispersion photographic spectra secured on two consecutive nights at Rozhen and concluded that they can be better reconciled with a short period of $1\overset{d}{.}1679$, probably identical to the photometric period. Harmanec (1987) collected all available RVs from several sources and showed that they could be folded with various periods and suggested that the star should not be considered a spectroscopic binary. He suspected that the RV curve derived by AL was a manifestation of long-term variations known for a number of other Be stars. Koubský et al. (2004) secured a new series of electronic spectra of *o* Cas with a good S/N. Measuring RVs of the steep wings of the Hα emission, they demonstrated that the RV variations are strictly periodic and therefore almost certainly due to orbital motion. They found $P = 1031$ d and $e = 0$. However, they were unable to explain why the lines of the secondary, probably more massive than the primary (as implied by the high mass function of 0.867 $M_\odot$), were unobservable. Jancart et al. (2005) analyzed the Hipparcos astrometric data and concluded that *o* Cas is undoubtedly an astrometric binary. Adopting the AL elliptical-orbit solution, they derived the astrometric orbit with a semi-major axis of $0\overset{''}{.}0074 \pm 0\overset{''}{.}0013$ and inclination $107\overset{\circ}{.}2 \pm 4\overset{\circ}{.}3$.

2. Observations and reductions

2.1. Spectroscopy

The star was observed in Ondřejov and later also at the Dominion Astrophysical Observatory (DAO hereafter). Altogether, we secured and reduced 442 usable electronic spectra covering the red spectral region around the Hα and He I 6678 lines. We measured RVs on the steep wings of the Hα emission line and also on the outer wings of the He I 6678 absorption line. We measured the peak intensity of the Hα emission to characterize the long-term changes of the envelope. Additionally, we compiled and analyzed several sets of RVs published by various authors as well as all available records of the peak intensity of the Hα emission. A journal of all RV observations is given in Table 1.

Details on data reduction and on RV and peak-intensity measurements can be found in Appendix A. In the same Appendix, readers can also find Table A.1 with HJDs and individual RVs compiled from the literature, Table A.2 with records of the peak intensity of the Hα emission compiled from the literature and public databases of the Be-star spectra, and Table A.3 with all Hα emission and He I 6678 absorption RVs and the Hα peak intensities measured in the electronic spectra.

2.2. Photometry

UBV: photometry has been carried out at Hvar since 1982. The measurements were carefully transformed to the standard Johnson *UBV* system via non-linear tranformation formulæ using the program HEC22 (Harmanec et al. 1994; Harmanec & Horn 1998). We also used the Hipparcos H_p broadband all-sky observations. To be able to combine them with the Hvar observations, we transformed them to the Johnson *V* magnitudes following Harmanec (1998). Additionally, we compiled all photometric observations from the literature which either were on or could be transformed to the Johnson *UBV* system. Basic information on available data sets with known times of observations can be found in Table 2.

We also compiled all-sky *UBV* observations without known times of observations, which are summarized in Table 3.

Table 1. Journal of RV data sets.

Spg. No.	Epoch (HJD-2 400 000)	No. of RVs	Source
1	17065.9–19290.8	5	A
2	20745.0–20796.9	4	B
3	24026.0–24769.0	7	C
4	41881.9–42724.7	20	D
5	37274.7–43101.8	6	E
6	22525	3	F
7	45980.4–45981.5	3	G
8	48813.5–51509.4	23	H
9	52280.4–54385.5	239	H
10	52695.3–52695.3	2	H
11	52706.7–54599.0	178	H

Notes. *Column "Spectrograph No.":* 1: Yerkes, Bruce 1-prism spg.; 2: Lick light 1-prism; 3: Dominion Astrophysical Observatory 1.83-m reflector, 1-prism spg., IL, IM, IS, ISS and IIM configurations; 4: Kitt Peak National Observatory, 1-m coudé auxiliary spg.; 5: MtWilson 1.5-m reflector, Cassegrain spg.; 6: Ottawa; 7: Rozhen 2.0-m reflector, coude grat. spg.; 8: Ondřejov 2.0-m reflector, coude grating spg., Reticon 1872RF detector; 9: Ondřejov 2.0-m reflector, coude grating spg., CCD detector; 10: Ondřejov 2.0-m reflector, Heros echelle spectrograph in the Cassegrain focus, CCD detector; 11: Dominion Astrohysical Observatory 1.22-m reflector, coude grating spg., SITE-4 4096 CCD detector.
Abbreviations of column "Source": A: Frost et al. (1926); B: Campbell & Moore (1928); C: Plaskett & Pearce (1931); D: Abt & Levy (1978); E: Elias et al. (1978); F: Henroteau (1921); G: Horn et al. (1985); H: this paper.

Details on photometric data sets and their reductions and transformations can be found in Appendix B.

2.3. Interferometry

The star was observed with the Navy Prototype Optical Interferometer (NPOI) located near Flagstaff, Arizona, during three successive observing seasons in 2005, 2006, and 2007. The NPOI was described by Armstrong et al. (1998) and measures interference fringe amplitudes and closure phases in 16 spectral channels between 550 nm and 850 nm, on baselines up to 64 m in length on the ground (for the observations reported here). The width of the channels ranges from 3% to 2% of the central wavelength from the red to the blue end of the spectrometer. The closure phase, corresponding to the sum of the visibility phase measured for each baseline in a triangle, is free of atmospheric phase fluctuations. The observations of *o* Cas were interleaved with a calibrator star, taken from a list maintained at NPOI. The calibrators, together with the values adopted for their uniform disk diameters at 800 nm (estimated uncertainty of 3%) and the predicted squared visibility at 800 nm on a 60 m baseline were κ And (0.37 mas, $V^2 = 0.96$), μ And (0.69 mas, $V^2 = 0.85$), and ζ Cas (0.26 mas, $V^2 = 0.98$). Diameters at other wavelengths were computed based on the appropriate amount of limb darkening. Dates of observation and other relevant information as well as astrometric fitting results discussed further below are listed in Table 4. The total *uv*-coverage achieved is shown in Fig. 1.

The reduction of the NPOI data followed the procedures described by Hummel et al. (1998), with the only difference that incoherent flux measurements (obtained by offsetting the optical delay lines) were done for each stellar fringe measurement in order to derive more precise estimates of the visibility amplitude bias due to non-Poisson detector statistics. The calibrator

Table 2. Journal of the photoelectric measurements with known times of observations.

Station No.	Epoch HJD-2 400 000	No. of obs. *U*/*B*/*V*	$HD_{comp.}$/ check	Passbands used	Source
23	38295.8–38310.8	3/3/3	all-sky	*UBV*	Johnson et al. (1966)
30	39745.9–44892.8	7	all-sky	m_{58}	Schuster & Guichard (1984); Mitchell & Johnson (1969)
26	40452.6–40458.6	2/2/2	all-sky	*UBV*	Haupt & Schroll (1974)
1	45212.6–51512.3	343/343/343	4142/6114	*UBV*	Pavlovski et al. (1997); Harmanec et al. (1997)
61	47867.7–49038.4	–/–/148	all-sky	*V*	Perryman & ESA (1997)
1	51943.3–55104.4	372/372/372	4142/6114	*UBV*	this paper

Notes. Abbreviations of column "Stations" (numbers are running numbers of the observing stations from the Ondřejov data archives): 01: Hvar Observatory, 0.65-m Cassegrain reflector; 61: Hipparcos H_p magnitude transformed to Johnson *V* after Harmanec (1998); 23: Catalina Observatory, 1P21 tube; 26: Chiran Station of the Haute Provence Observatory, 0.60-m reflector, Lallemand tube; 30: San Pedro Mártir, 0.84 & 1.5-m reflectors.

Table 3. Published all-sky *UBV* observations with unknown epoch.

JD– 2 400 000	*V*	*B* − *V*	*U* − *B*	Source
?	4.62	−0.08	−0.49	Crawford et al. (1971)
?	4.55	−0.06	–	Bouigue (1959)
35960–36260	–	−0.064	−0.505	Belyakina & Chugainov (1960)
35450–36300	4.60	−0.07	−0.51	Mendoza (1958)
37300–37840	4.59	−0.079	−0.495	Crawford (1963)
38516–39095	4.45	−0.058	–	Häggkvist & Oja (1966)

Notes. Whenever possible, we estimated at least a range of Julian dates within which the particular observations were secured.

Table 4. NPOI observations and model fit results.

UT Date	Julian Year	Triangles	Calibrator	ρ [mas]	θ [deg]	σ_{maj} [mas]	σ_{min} [mas]	PA [deg]
2005 Sep. 13	2005.6996	EC-W7C-W7E	κ And	9.5	134.3	0.58	0.10	120
2005 Sep. 15	2005.7051	EC-W7C-W7E	κ And	10.1	132.4	0.55	0.09	119
2006 Nov. 18	2006.8796	EC-W7C-W7E, W7C-CW-W7W	μ And	7.5	19.5	0.47	0.11	95
2007 Aug. 9	2007.6024	EC-NC-EN, E6E-E6N-EN	ζ Cas	16.8	270.4	0.54	0.15	46
2007 Aug. 18	2007.6271	EC-NC-EN, E6E-E6N-EN	ζ Cas	17.0	268.1	0.52	0.16	38
2007 Aug. 20	2007.6326	EC-NC-EN, E6E-E6N-EN	ζ Cas	16.9	269.1	0.57	0.15	46

Notes. The listed triangles of baselines refer to the astrometric stations E (East), C (Center), W (West), and N (North), and the imaging stations W7 and E6. ρ and θ (measured east from north) refer to the position of the secondary relative to the primary component. σ_{maj} and σ_{min} and PA refer to the major, minor axis, and position angle of the error ellipse of the position measurement. The shape and orientation of this error ellipse is directly related to the synthesized beam.

visibility measurements were smoothed in time with a Gaussian kernel of 80 min in length to interpolate values at the epochs of the *o* Cas measurements. While the amplitudes of *o* Cas were thus calibrated by division, closure phases were calibrated by subtraction of the interpolated calibrator phases. We computed calibration uncertainties by the scatter of the calibrator measurements around the smoothed values, and they ranged from 5% to 20% for the amplitudes from the red to the blue end of the spectrometer, while they were typically around one or two degrees for the closure phases. Instead of applying the calibration error to the formal visibility errors, we allowed the mean level of the amplitude on individual baselines to float up or down a few percent to improve the fits (described below). This procedure is based on the observation that channel-to-channel variations of the visibility amplitude are not affected by a calibration error and therefore must be preserved, as they contain calibration independent visibility information.

The image of *o* Cas shown in Fig. 2 was obtained with standard interferometric phase self-calibration techniques, and shows for the first time the companion. As an example of the calibrated visibilities we obtained, Fig. 3 shows data from 2007 Aug. 9.

3. Spectroscopic and interferometric-orbit solutions

3.1. Radial velocities

Similarly as for some other Be stars, we measured the radial velocity on the steep wings of the Hα emission line comparing the direct and flipped line profiles in the program SPEFO (Horn et al. 1996; Škoda 1996). Because the Hα emission of *o* Cas during the time interval covered by our spectra reached peak intensities four to six times higher than the continuum level, these measurements are very accurate.

Figure 4 shows a plot of these emission RVs vs. time. One can see a clear periodic pattern of variations but there is also a hint of mild long-term changes. This was confirmed by trial

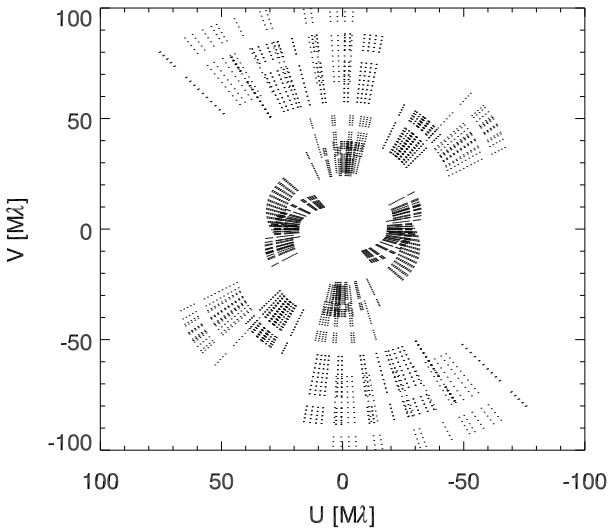

Fig. 1. *uv*-coverage achieved from the combined NPOI observations.

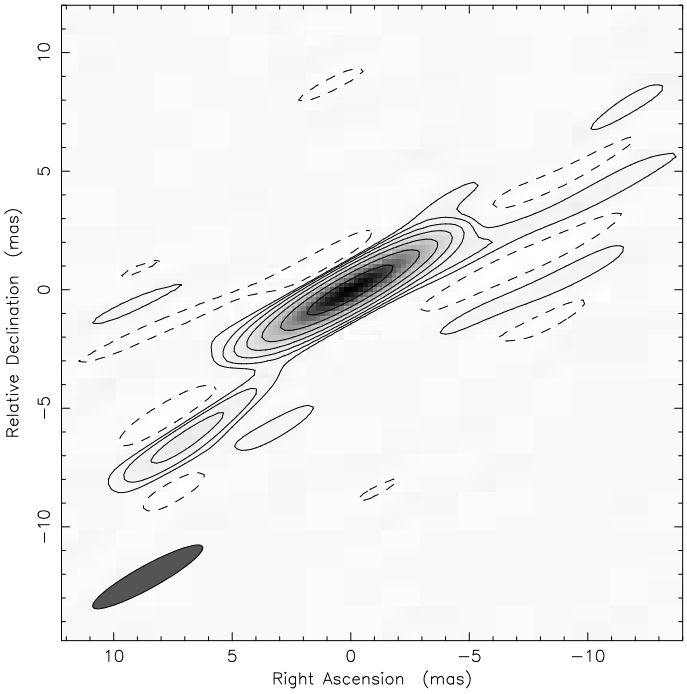

Fig. 2. Image of Omicron Cassiopeiae from the NPOI data of 2005 Sep. 15. Equidistant (logarithmically) contours start at 1.02% and end at 65.3%, the dashed contour denotes a level of −1.02%. The restoring beam size is shown in the lower left corner.

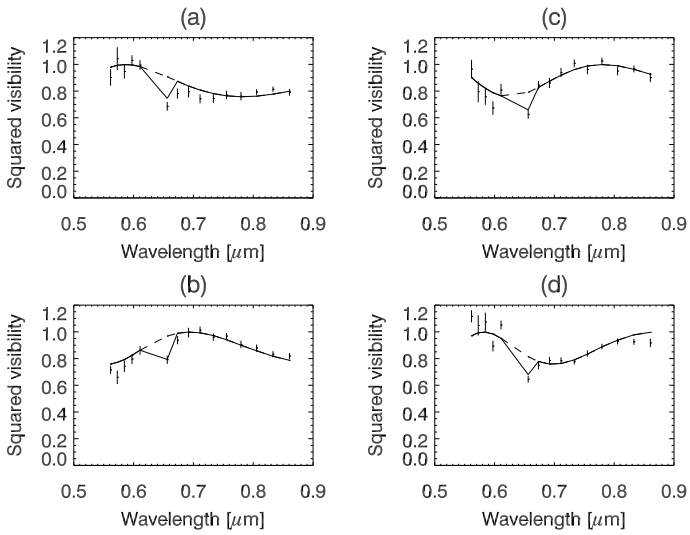

Fig. 3. Calibrated (squared) visibility amplitudes plotted versus wavelength for 2007 Aug. 9, on the AE-AN baseline at 10:18, 10:49, 11:17, and 11:53 UT. The solid line shows the model prediction for a fit with component separation $\rho = 17$ mas and PA $\theta = 270°$. The amplitude of the quasi-sinusoidal amplitude variation is fit with a magnitude difference $\Delta m = 2.9$. The dashed line shows the prediction of a model without the H-α disk.

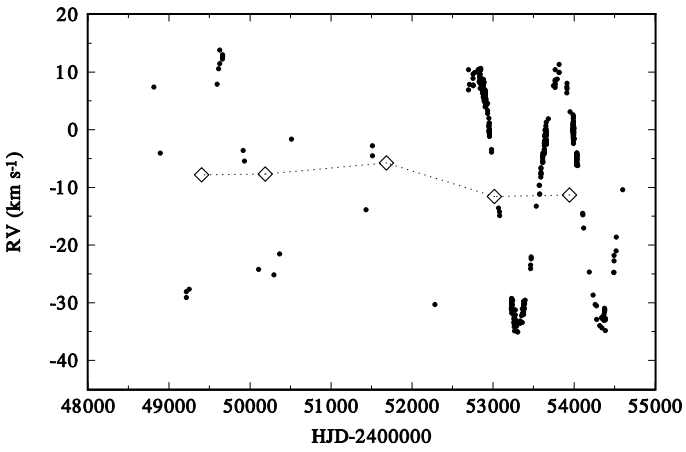

Fig. 4. RVs measured on the steep wings of the Hα emission line plotted vs. epoch of observation. A periodic variation as well as mild long-term changes are seen. The diamonds indicate mean (systemic) velocities for the five subsets of data (see text).

phase plots for the known 1030-d period. Such long-term variations are also known for some other Be stars which were found to be spectroscopic binaries: γ Cas (Harmanec et al. 2000; Harmanec 2002) may serve as a good example. To cope with this problem, we divided the RVs into five time intervals, each covering not more than about 1000 days, and allowed the program FOTEL for the orbital solution (Hadrava 1990, 2004) to derive individual mean (systemic) velocities for these subsets. This led to a very good fit (adopting a value of zero for the eccentricity) given as solution 1 in Table 5. The corresponding orbital RV curve is shown in Fig. 5 and the ephemeris for the 1032-d period reads:

$$T_{\mathrm{RV\,max}} = (\mathrm{HJD}\,2\,451\,759.2 \pm 1.4) + (1031\overset{\mathrm{d}}{.}55 \pm 0\overset{\mathrm{d}}{.}71) \times E. \quad (1)$$

Just to demonstrate how accurate our RV measurements of the Hα line are, we subjected the O–C deviations from the orbital solution 1 to a period search over the range of periods from 5000 d down to 0.5 d. The strongest signal was found at a period of $1\overset{\mathrm{d}}{.}2578$ which is the period known from photometry prewhitened to compensate the long-term changes. A formal sinusoidal fit for this period is tabulated in Table 6 and the corresponding phase diagram is in Fig. 6.

As seen in the bottom panel of Fig. 5, the RVs of the presumably photospheric He I 6678 line exhibit much larger scatter than that of the Hα emission wings, clearly due to strong line-profile variations. It is encouraging, however, that the orbital solution for the He I 6678 RVs does not contradict that from the more accurate emission RVs.

We also computed several orbital solutions in which we tried to combine our new Hα emission line RVs with RVs published in the literature – see Table A.1 – to see if we could improve the

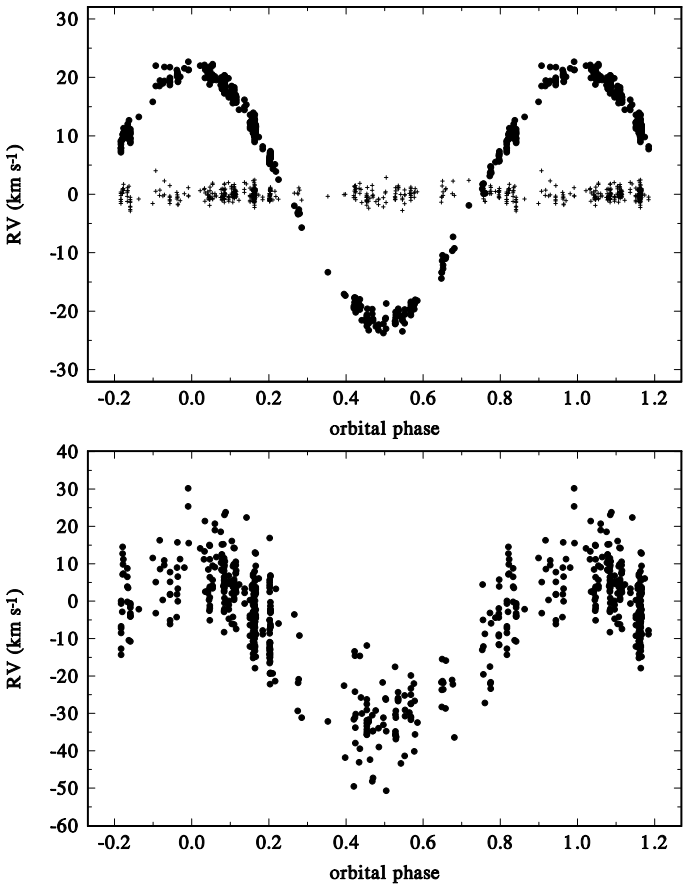

Fig. 5. Phase diagram for the 1031-d period as defined by ephemeris (1). The RVs in *the upper panel* were measured on the steep wings of the Hα emission line and prewhitened to compensate the long-term changes. The crosses indicate the O–C deviations from the orbital solution. *The lower panel* shows RVs measured on the absorption line He I 6678. See the text for details.

Table 5. The (circular) orbital solutions based on the 1031-d period.

Element	Solution 1: Hα emis.	Solution 2: He I 6678
P (d)	1031.55 ± 0.71	1031.55 fixed
$T_{\mathrm{RV\,max}}$	51759.2 ± 1.4	51749.5 ± 4.5
K (km s^{-1})	21.593 ± 0.071	20.81 ± 0.60
γ (km s^{-1})	*)	−12.36 ± 0.41
$f(m)$ ($M_\odot$)	1.076	0.9634
rms (km s^{-1})	0.944	7.42
No. of RVs	437	430

Notes. For the Hα emission line RVs, the data were divided into five segments, covering individual orbital periods, and treated formally as coming from different spectrographs with different systemic RVs. Thus, we were able to remove the slight long-term variations affecting the RVs. No such procedure was applied to the He I 6678 RVs. All epochs are in HJD-2 400 000; rms is the rms of the O–C values.
*) Local γ's ranged from −5.8 to −11.6 km s^{-1}, all with rms errors below 1 km s^{-1}.

value of the orbital period. Regrettably, the lower accuracy and heterogeneity of the published RVs did not allow that. Therefore, we show in Fig. 7 only a phase diagram for our preferred period of 1031$^{\mathrm{d}}$.55 for all RVs from the literature to demonstrate that these older observations are also in phase with our more recent RV data. Considering the above arguments, our subsequent analysis of binary masses will be based on the orbital solution 1.

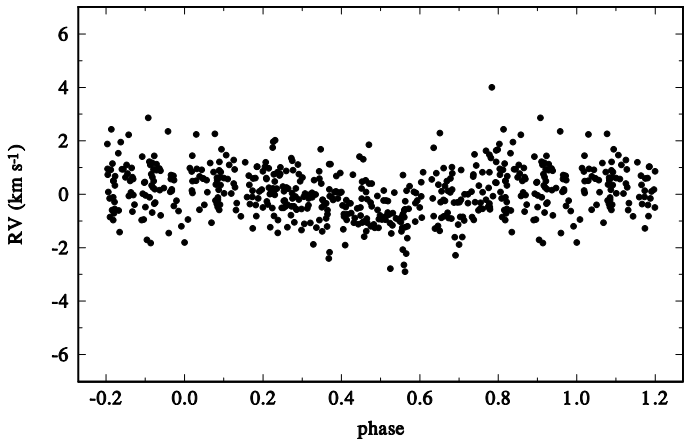

Fig. 6. Phase diagram for the 1$^{\mathrm{d}}$.2578 period as defined by ephemeris of Table 6. It is based on the O–C residuals from the fit to the Hα emission line RVs prewhitened after removal of the long-term changes. See the text for details.

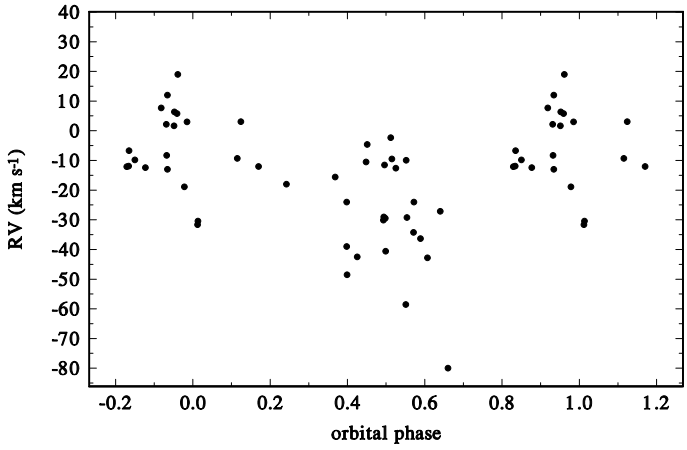

Fig. 7. Phase diagram for the old RVs from the literature for the the orbital solution for the Hα emission wings given in Table 5.

Table 6. A sinusoidal fit for the 1.2578-d period in the Hα emission RV O–C residuals.

Element	Value
P (d)	1.257805 ± 0.000029
$T_{\mathrm{RV\,max}}$	51808.812 ± 0.042
K (km s^{-1})	0.52 ± 0.30
rms (km s^{-1})	0.869

Notes. K is the semiamplitude of the curve and rms is the rms error of one observation.

3.2. Interferometric orbit and the basic physical properties of the system

As shown in Fig. 3, both the relative position of the binary components as well as their magnitude difference can be extracted from the data collected in each night. The astrometric results are reported in Table 4 and were used to fit the inclination i of the orbit, the angle of the ascending node Ω, and the semimajor axis a, adopting the remaining elements from the spectroscopic orbit. This orbit is shown in Fig. 8. The results were finally confirmed by fitting all component parameters, including their masses, and orbital elements to the interferometric data (reduced $\chi^2_{\mathrm{r}} = 1.9$) and the radial velocities (reduced $\chi^2_{\mathrm{r}} = 1.0$ adopting 1 km s^{-1} for

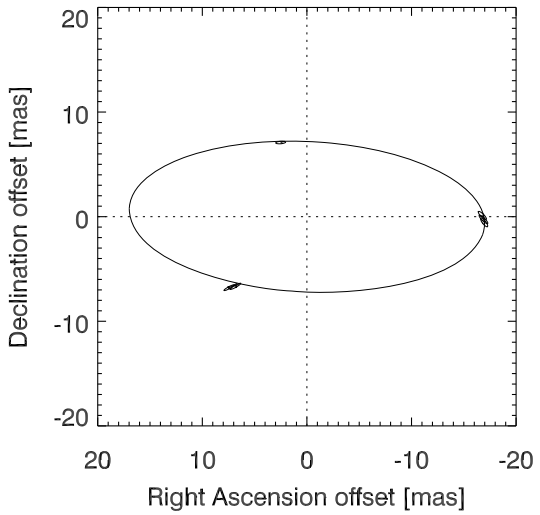

Fig. 8. Apparent orbit of o Cas from interferometry and spectroscopy. The size of the uncertainty ellipses are set to one-fifth of the synthesized beam widths.

Table 7. Orbital elements from combined fits.

Parameter	Solution
P	$1031^{\rm d}.55$ (fixed)
T	JD 2452792.2 ± 0.6
a	$0''.0170 \pm 0''.0006$
i	$115^\circ.0 \pm 2^\circ.6$
Ω (2000.0)	$267^\circ.3 \pm 0^\circ.8$
Δm (700 nm)	$2^{\rm m}.9 \pm 0^{\rm m}.1$

the uncertainty of a measurement) using procedures described in Hummel et al. (1998). If one adopts the original Hipparcos parallax of $0''.00360 \pm 0''.00084$ (Perryman & ESA 1997), it is also possible to estimate the individual masses, giving $\mathcal{M}_1 = 6.9\ M_\odot$ and $\mathcal{M}_2 = 6.3\ M_\odot$, but the uncertainties due to the error of the parallax are rather large. van Leeuwen (2007a) reanalyzed the Hipparcos data and obtained a parallax of $0''.00464 \pm 0''.00038$ (van Leeuwen 2007b). This would imply much lower masses of $\mathcal{M}_1 = 2.4\ M_\odot$ and $\mathcal{M}_2 = 3.8\ M_\odot$ for primary and secondary components, respectively. Despite the uncertainties in these values, the conclusion of Koubský et al. (2004) that the companion must have a mass comparable to, or even higher than the much brighter Be primary, remains unaltered.

Both determinations of the parallax from the Hipparcos data accounted for the motion of the binary, and resulted in values of the semimajor axis of the orbit of the photo center, a_0, as well as the inclination and angle of the line of nodes when the remaining elements were adopted from the spectroscopic orbit. While Jancart et al. (2005) published a value of $a_0 = 7.4 \pm 0.4$ mas, we repeated this analysis based on the new Hipparcos reduction by van Leeuwen (2007b) and our new spectroscopic orbit, and confirmed a nearly circular orbit with $a_0 = 7.8 \pm 0.4$, $\Omega = 275^\circ$, and $i = 103^\circ$. These results provide an additional constraint as they can be computed from the component mass ratio and magnitude difference and from the semimajor axis of the orbit.

Therefore we determined with Kepler's third law and the measured mass function, that a parallax of 3.7 ± 0.2 mas would yield values for a_0 consistent with Jancart et al. (2005) and our own analysis. In addition, only in this range would the stellar classes of the primary corresponding to the determined mass ($\mathcal{M}_1 = 6.2\ M_\odot$) and absolute magnitude ($M_V = -2^{\rm m}.6$) match.

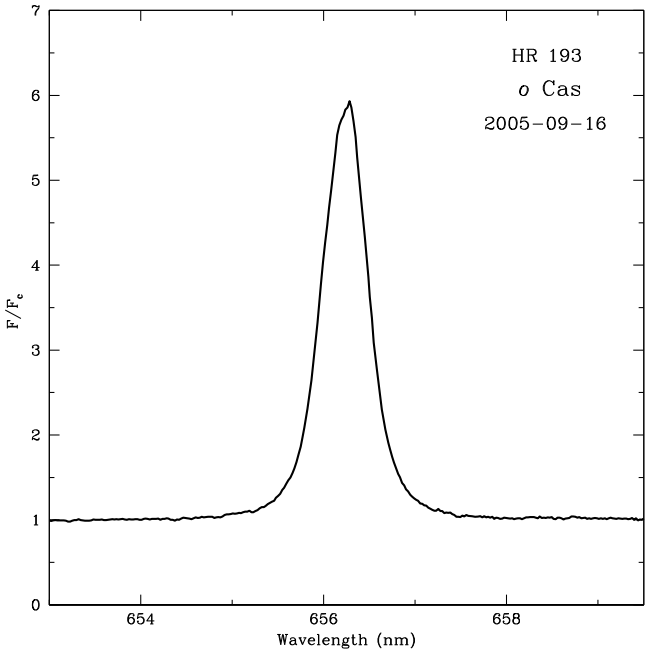

Fig. 9. Hα line profile normalized with repect to the continuum, obtained on 2005 Sep. 16 (JD 2 453 630).

The secondary, however, is always too massive for being almost 3 mag fainter than the primary. A possible solution to this problem will be discussed later in this paper.

Because both giant B5 and dwarf B3 stars have masses consistent with our results, we adopted the following approach. Because the visual companion was found to be $2^{\rm m}.9$ fainter than the Be primary, one can use the *UBV* magnitudes from the time interval when the star was without emission $V = 4^{\rm m}.61$, $B - V = -0^{\rm m}.075$, $U - B = -0^{\rm m}.525$ (see Table B.2) to obtain dereddened values $V_0 = 4^{\rm m}.35$, $(B - V)_0 = -0^{\rm m}.156$, and $(U - B)_0 = -0^{\rm m}.584$. These values corresponds well to a B5 star and to an effective temperature of 14 000 K according to the calibration by Flower (1996). From the magnitude difference of $2^{\rm m}.9$, one obtains the dereddened visual magnitude of the primary $V_0^1 = 4^{\rm m}.42$. Adopting $\log T_{\rm eff} = 4.145$ and B.C. $= -1^{\rm m}.05$ after Flower (1996) and the parallax of $0''.0037$, one arrives at $M_V = -2^{\rm m}.55$ and $R = 8.0\ R_\odot$, which agrees well with the spectral classification B5III.

4. Circumstellar disk

4.1. Interferometric signature

The dip in the visibility amplitudes at 660 nm (see Fig. 3) is caused by the extended Hα emission around the primary. To visualize this effect for all data from the NPOI channel centered on the Hα line we divided the observed visibility amplitudes by the those predicted with the binary model, which left a single unresolved component and the envelope. (This is an approximation, but because the closure phases are never larger than about 10 degrees and the secondary is almost 3 mag fainter than the primary, it is a good one.) The resulting amplitudes as a function of *uv*-radius are shown in Fig. 10.

In order to determine the size of this envelope and any apparent flattening, we used the Hα line profile (Fig. 9) to estimate the fraction of Hα emission relative to the continuum in the NPOI spectral channel centered on the line. The line profile was measured with a fiber-fed echelle spectrograph connected to the John S. Hall 1.1-m telescope at the Lowell Observatory. The spectra

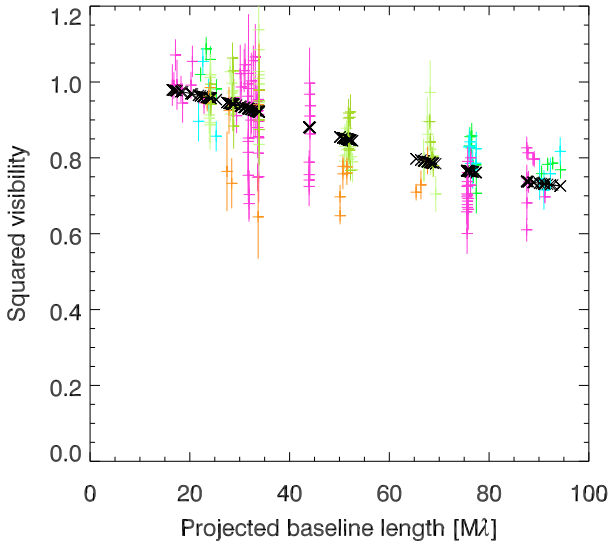

Fig. 10. Observed visibility amplitudes (Hα channel only) divided by the binary model predictions for all NPOI data. Model values of a Gaussian component with *FWHM* of 1.9 mas and 24% flux contribution to the continuum flux in the Hα channel are also shown.

in the Hα line region were reduced using standard reduction routines developed by Hall et al. (1994) and had a spectral resolving power of 10 000. The equivalent width of the line was measured to be 3.3 nm, or 22% of the width of the NPOI channel containing the line. To correct for the effect of the Hα absorption of the star itself, we estimated an equivalent width of about 0.26 nm, or 1.7% of the NPOI channel based on a stellar atmosphere model with $T = 14\,000$ K and $\log(g) = 3.8$. Therefore the total emission of the disk will be slightly larger, i.e. about 3.6 nm, or 24% of the NPOI channel. It would be possible, as demonstrated by Tycner et al. (2006), to disentangle the fractional flux contributed by the line to the total flux measured in the channel from the diameter with better data on longer baselines, where the amplitudes should reach asymptotically a value of $(1/1.24)^2 = 65\%$ based on our results.

Following Tycner et al. (2006, 2008), we adopt a circular Gaussian component representing the disk emission and fit a diameter of 1.9 ± 0.1 mas to (non-divided) the Hα data using the complete model including the binary. The reduced $\chi^2_r = 3.0$ of the fit indicates that substructure exists within the disk that is not fitted by a circular Gaussian component. If we allow an elongation of the component, an axial ratio of 0.6 with the major axis of an ellipse oriented roughly in a north-south direction allows us to improve the fit to $\chi^2_r = 2.5$. However, at this position angle, the axial ratio is only weakly constrained due to the lack of long baselines in east-west direction (see Fig. 1). If we assumed instead a position angle of 90 degrees, our data would not allow an axial ratio of less than about 0.8 ($\chi^2_r = 3.4$), corresponding to an inclination of the disk normal to the line of sight of not more than 36 degrees assuming the disk has a narrow opening angle and is itself circular.

The quality of our H_α data due to the limits imposed by the *uv*-coverage and the dilution of the emission with the stellar continuum given the width of the NPOI channel does not allow further conclusions except to say that a nearly face-on disk is consistent with our data. At the same time, a disk aligned with the orbital plane is inconsistent with our observations, unless a very wide disk opening angle is assumed.

4.2. Correlated spectroscopic and photometric signatures

As pointed out already by Harmanec (1983), Be stars usually vary on three distinct time scales: long-term (years to decades), medium (weeks to months), and rapid (less than about two days). The variations on the two shorter time scales are often periodic, related to the binary nature and to the stellar rotation and/or pulsations, respectively. Because all these periods may be present in a particular star, it is necessary to obtain a very dense and complete observational coverage to be able to remove the non-periodic long-term changes and to search for periodic components of the variations.

o Cas is an example of a Be star with pronounced changes on all these timescales. In Fig. 11 we show a plot of several observed quantities as a function of time: individual photometric observations of the Johnson V magnitude and $B-V$ and $U-B$ indices, and the peak intensity of the Hα emission line. This diagram covers the time interval for which photoelectric observations are available. The color–color diagram for all individual observations for the same time interval is shown in Fig. 12. It is obvious that the mutual correlation between the emission strength, brightness and colors is rather complicated and obviously governed by at least two different processes.

1. The formation of each new emission-line episode (like the one which occurred around JD 2 439 000) is indicative of *the positive correlation* between the brightness of the object and the emission strength (Harmanec 1983, 2000). In the color–color diagram the object moves from the main sequence towards supergiants. According to Harmanec (1983) this indicates that the inner, optically thick parts of the disk simulate a stellar photosphere which increases its radius. If such a *pseudophotosphere* is seen not just equator-on but under some smaller angle, it mimics an increase of the luminosity class of the star in the $U-B$ vs. $B-V$ diagram, which is indeed observed.
2. In the time interval between about JD 2 447 000 and 51 000, the increase of the emission strength continues but the brightness of the object started to decrease again. This is not a mere effect of the change of the emission (ratio ~1.7) due to the continuum change (ratio ~1.15). This can be qualitatively interpreted as a gradual rarification of the envelope, which becomes more extended but optically thin in continuum, which means that the radius of the pseudophotosphere is decreasing again. A remarkable variation occurs around JD 2 452 000 when the brightness rises again while at the same time both color indices drop sharply (the object gets redder) and the emission strength also decreases temporarily.

In any case, an important finding is that over the whole period of our spectral and interferometric observations, the circumstellar envelope was strong and relatively stable (peak normalized intensities between about 4 and 6–7).

4.3. Evidence for phase-locked changes

We attempted to remove the long-term peak-intensity variations from our homogeneous observations with the program HEC13, which is based on a fit via spline functions after Vondrák (1969, 1977)[2]. After a few experiments, we used the smoothing parameter $\varepsilon = 1 \times 10^{-14}$ through the 20-day moving box-car averaged data points as the optimal choice. A period analysis of the

[2] The program HEC13 with simple instructions for use is freely available at http://astro.troja.mff.cuni.cz/ftp/hec/HEC13.

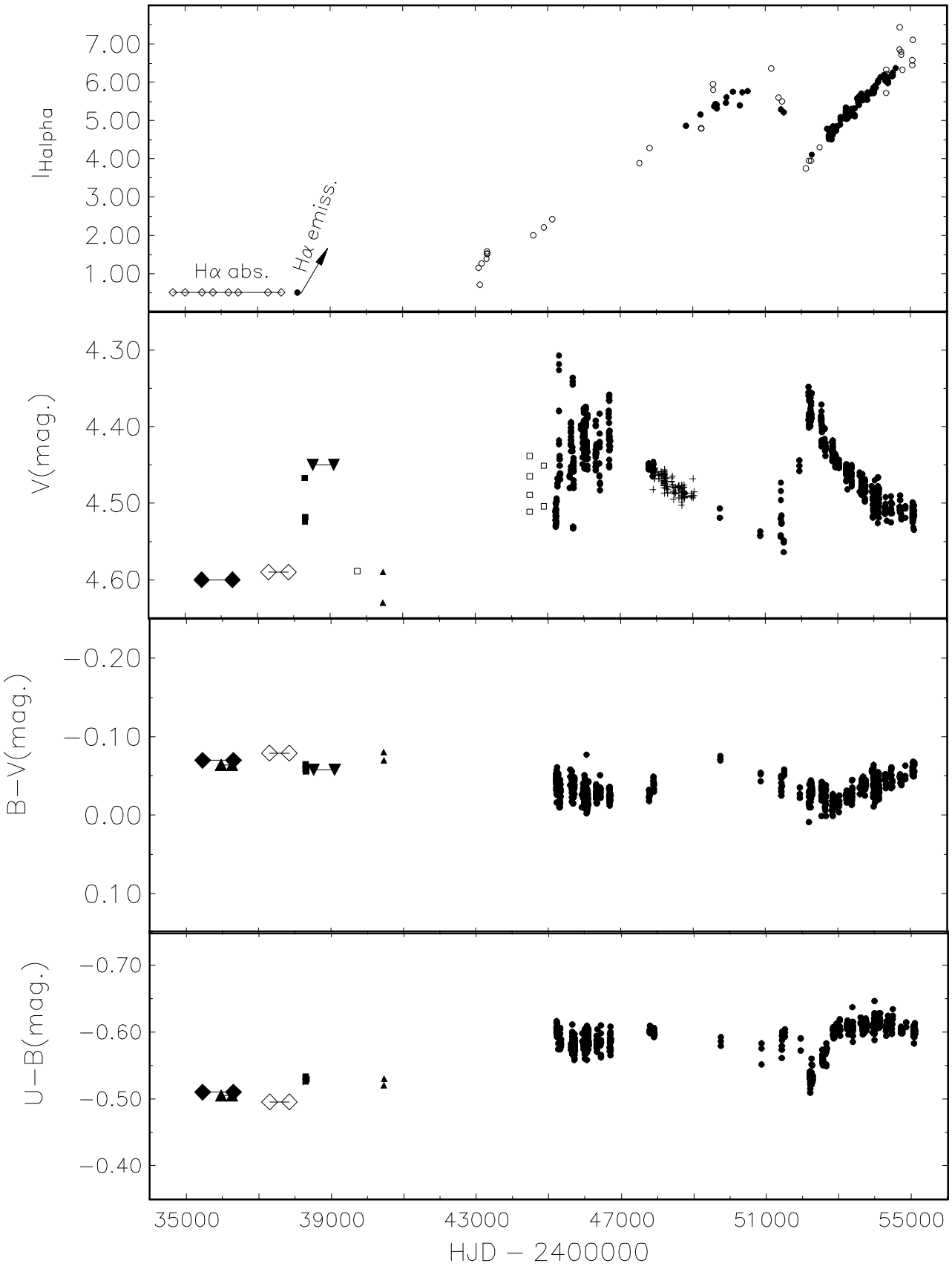

Fig. 11. Long-term variations seen in the peak intensity of the Hα emission, the V magnitude of the object, and $B - V$ and $U - B$ colours. Filled circles denote our observations, open circles the Hα peak intensities compiled from the literature, + – Hipparcos photometry, filled squares – Johnson et al. (1966), open squares – the m_{58} photometry, filled triangles (up) – the all-sky *UBV* photometry by Haupt & Schroll (1974), filled triangles (down) – Häggkvist & Oja (1966), filled diamonds – Mendoza (1958), open diamonds – Crawford (1963).

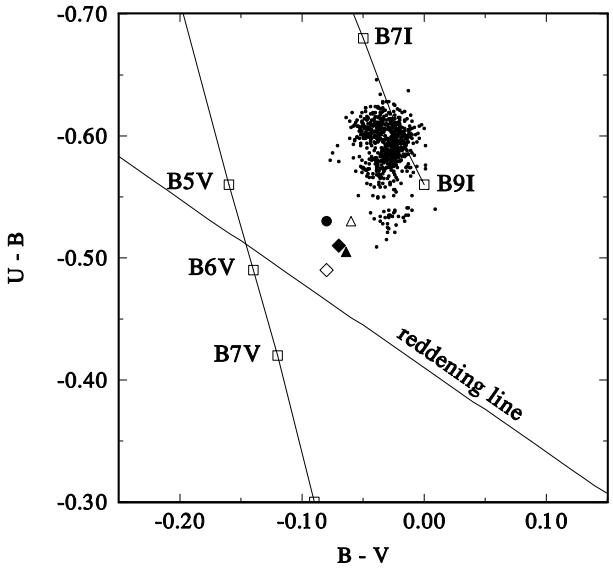

Fig. 12. Long-term variations of *o* Cas in the two-color diagram. They are characteristic for the positive correlation between the brightness and emission strength.

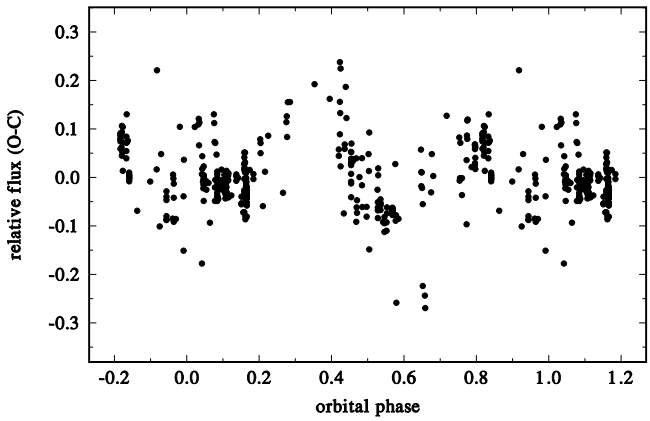

Fig. 13. Phase diagram for the residual Hα peak intensity prewhitened to compensate the long-term changes for the orbital period as defined by ephemeris (1). There is a hint of a double-wave curve with minima at both elongations of the binary.

O–C deviations from this fit clearly indicated the orbital period of 1032 d. The corresponding phase plot is shown in Fig. 13 and seems to indicate a double-wave variation with minima centered on the binary elongations.

5. Discussion

An important issue we have to address is the contradiction, now confirmed, of a secondary of nearly the same mass as the primary, but which is, however, 3 mag fainter. As already pointed out by Koubský et al. (2004), the large mass function is inconsistent with the absence of any discernable lines from the secondary. One possibility we will discuss here is *the binary nature of the secondary itself*. If we adopt an absolute magnitude $M_V = -2^{\rm m}.55$ for the primary (see Sect. 3.2), the observed magnitude difference of $2^{\rm m}.9$ implies $M_V = 0^{\rm m}.35$ for the companion. If the companion is indeed formed by two identical stars in a close binary orbit, each of these stars will be about $0^{\rm m}.7$ fainter in V, having $M_V = 1^{\rm m}.05$. According to the tabulation by Harmanec (1988), this corresponds to two early A dwarfs. Their combined mass can easily be something like 5 $M_\odot$, in agreement with our tentative estimate for the mass of the companion in Sect. 3.2. The hypothesis that the companion is a close binary is therefore internally consistent and seems to provide a solution to the problem of its seemingly large mass following from the orbital solution.

As to the size of the secondary binary, all we can say is that it must be unresolved with respect to the interferometric resolution of our observations. A possible example can easily be found in the double star β Aurigae (Hummel et al. 1995), which consists of two identical A2V components in a circular orbit of about four days period, and with a separation of 0.08 AU. If placed at the distance of *o* Cas, the apparent separation would be merely 0.3 mas. Only very high- resolution observations with future interferometers would be able to provide confirmation.

A second issue is that if the Hα emission region is formed in a disk, it cannot be coplanar with the orbit as indicated by its nearly circular apparent shape. This conclusion only holds if the disk is assumed to be geometrically thin (as suggested by some studies, see for example the list of references in Sect. 4.1 of Porter & Rivinius 2003). Otherwise coplanarity would imply a wide opening angle (several tens of degrees) of the circumstellar disk. If we assume the stellar spin axis is orthogonal to the disk plane, the maximum allowed angle of the disk normal to the line of sight of 36 degrees would translate into a rotation speed of 375 km s^{-1} at the equator derived from the measured $v \sin i = 220$ km s^{-1}. Note that for the mass of 6.2 $M_\odot$ and radius of 8.0 $R_\odot$ estimated in Sect. 3.2, the break-up velocity would be 390 km s^{-1}. Identifying the period of photometric and residual RV variability of 1.257-d with the stellar rotational period would imply an equatorial radius of 9.3 $R_\odot$, which generally agrees with our estimate of 8 $R_\odot$. Though the range of uncertanties is broad, there is a serious possibility that the Be primary is close to the break-up speed. Surface features away from the pole could create the photometric variability, and the radial velocity variation via line profile variations.

Acknowledgements. We acknowledge the use of the latest publicly available version of program FOTEL written by Dr. Petr Hadrava. We also gratefully acknowledge the use of several spectra of *o* Cas made available in the Be Star Spectra (BeSS) database maintained at the Paris-Meudon Observatory and a few additional publicly available spectra secured by Mr. C. Buil at his private observatory. Dr. H. F. Haupt kindly provided PH with two individual *UBV* observations of *o* Cas. Our thanks are also due to Drs. P. Hadrava, M. Wolf, P. Škoda, S. Štefl, V. Votruba and Ms. A. Budovičová and Mr. P. Chadima who obtained several spectra and *UBV* observations used in this study. The authors would also like to thank Jim Benson and the NPOI observational support staff whose efforts made this project possible. This research was supported by the grants 205/03/0788, 205/06/0304, 205/08/H005 and P209/10/0715 of the Czech Science Foundation, from the research project AV0Z10030501 of the Academy of Sciences of the Czech Republic and from the Research Program MSM0021620860 *Physical study of objects and processes in the solar system and in astrophysics* of the Ministry of Education of the Czech Republic. The research of P.K. was supported from the ESA PECS grant 98058. C.T. acknowledges, with thanks, grant support from Research Corporation for Science Advancement and the Central Michigan University. The Navy Prototype Optical Interferometer is a joint project of the Naval Research Laboratory and the US Naval Observatory, in cooperation with Lowell Observatory, and is funded by the Office of Naval Research and the Oceanographer of the Navy. We acknowledge the use of the electronic database from CDS Strasbourg and electronic bibliography maintained by the NASA/ADS system. We are very grateful to an anonymous referee for a prompt and encouraging report, with useful comments and suggestions which helped to improve the manuscript.

References

Abt, H. A., & Levy, S. G. 1978, ApJS, 36, 241
Andrillat, Y., & Fehrenbach, C. 1982, A&AS, 48, 93

Armstrong, J. T., Mozurkewich, D., Rickard, L. J., et al. 1998, ApJ, 496, 550
Banerjee, D. P. K., Rawat, S. D., & Janardhan, P. 2000, A&AS, 147, 229
Barker, P. K. 1983, PASP, 95, 996
Belyakina, T. S., & Chugainov, P. F. 1960, Izvestiya Ordena Trudovogo Krasnogo Znameni Krymskoj Astrofizicheskoj Observatorii, 22, 257
Bouigue, R. 1959, Annales Obs. Astron. Meteo. Toulouse, 27, 47
Campbell, W., & Moore, J. 1928, Publ. Lick Obs., 16, 1
Crawford, D. L. 1963, ApJ, 137, 523
Crawford, D. L., Barnes, J. V., & Golson, J. C. 1971, AJ, 76, 1058
Elias, J., Lanning, H., & Neugebauer, G. 1978, PASP, 90, 697
Flower, P. J. 1996, ApJ, 469, 355
Frost, E. B., Barrett, S. B., & Struve, O. 1926, ApJ, 64, 1
Hadrava, P. 1990, Contribut. Astron. Obs. Skalnaté Pleso, 20, 23
Hadrava, P. 2004, Publ. Astron. Inst. Acad. Sci. Czech Rep., 92, 1
Häggkvist, L., & Oja, T. 1966, Arkiv Astron., 4, 137
Hall, J. C., Fulton, E. E., Huenemoerder, D. P., Welty, A. D., & Neff, J. E. 1994, PASP, 106, 315
Harmanec, P. 1983, Hvar Obs. Bull., 7, 55
Harmanec, P. 1987, Bull. Astron. Inst. Czech., 38, 283
Harmanec, P. 1988, Bull. Astron. Inst. Czech., 39, 329
Harmanec, P. 1998, A&A, 335, 173
Harmanec, P. 2000, in The Be Phenomenon in Early-Type Stars, ed. M. A. Smith, H. F. Henrichs, & J. Fabregat, IAU Colloq. 175, ASP Conf. Ser., 214, 13
Harmanec, P. 2002, in Exotic Stars as Challenges to Evolution, ASP Conf. Ser., 279, 221
Harmanec, P., & Horn, J. 1998, J. Astron. Data, 4, 5
Harmanec, P., Horn, J., & Juza, K. 1994, A&AS, 104, 121
Harmanec, P., Pavlovski, K., Božić, H., et al. 1997, J. Astron. Data, 3, 5
Harmanec, P., Habuda, P., Štefl, S., et al. 2000, A&A, 364, L85
Haupt, H. F., & Schroll, A. 1974, A&AS, 15, 311
Henroteau, F. 1921, Publ. Dominion Obs. Ottawa, 5, 45
Horn, J., Koubský, P., Božić, H., & Pavlovski, K. 1985, Info. Bull. Variable Stars, 2659, 1
Horn, J., Kubát, J., Harmanec, P., et al. 1996, A&A, 309, 521
Hubert, A. M., & Floquet, M. 1998, A&A, 335, 565
Hubert-Delplace, A.-M., & Hubert, H. 1979, An atlas of Be stars (Paris-Meudon Observatory)
Hummel, C. A., Armstrong, J. T., Buscher, D. F., et al. 1995, AJ, 110, 376
Hummel, C. A., Mozurkewich, D., Armstrong, J. T., et al. 1998, AJ, 116, 2536
Jancart, S., Jorissen, A., Babusiaux, C., & Pourbaix, D. 2005, A&A, 442, 365
Johnson, H. L., Iriarte, B., Mitchell, R. I., & Wisniewski, W. Z. 1966, Commun. Lun. Planet. Lab., 4, 99
Kaufer, A. 1988, Rev. Mod. Astrophys., 11, 177
Koubský, P., Ak, H., Harmanec, P., Yang, S., & Božić, H. 2004, in Variable Stars in the Local Group, ed. D. W. Kurtz, & K. R. Pollard, IAU Colloq. 193, ASP Conf. Ser., 310, 387
Mendoza, E. E. 1958, ApJ, 128, 207
Mitchell, R. I., & Johnson, H. L. 1969, Commun. Lun. Planet. Lab., 8, 1
Pavlovski, K., Harmanec, P., Božić, H., et al. 1997, A&AS, 125, 75
Perryman, M. A. C., & ESA. 1997, The HIPPARCOS and TYCHO catalogues, Astrometric and photometric star catalogues derived from the ESA Hipparcos Space Astrometry Mission (Noordwijk, Netherlands: ESA Publications Division), ESA SP Ser., 1200
Peton, A. 1972, A&A, 18, 106
Plaskett, J. S., & Pearce, J. A. 1931, Publ. Dominion Astrophys. Obs. Victoria, 5, 1
Porter, J. M., & Rivinius, T. 2003, PASP, 115, 1153
Richardson, E. H. 1968, JRASC, 62, 313
Schuster, W. J., & Guichard, J. 1984, Rev. Mex. Astron. Astrofis., 9, 141
Škoda, P. 1996, in Astronomical Data Analysis Software and Systems V, ASP Conf. Ser., 101, 187
Slettebak, A., & Reynolds, R. C. 1978, ApJS, 38, 205
Slettebak, A., Collins, II, G. W., & Truax, R. 1992, ApJS, 81, 335
Tycner, C., Gilbreath, G. C., Zavala, R. T., et al. 2006, AJ, 131, 2710
Tycner, C., Jones, C. E., Sigut, T. A. A., et al. 2008, ApJ, 689, 461
van Leeuwen, F. (ed.) 2007a, in Hipparcos, the New Reduction of the Raw Data, Astrophysics and Space Science Library, vol. 350
van Leeuwen, F. 2007b, A&A, 474, 653
Vondrák, J. 1969, Bull. Astron. Inst. Czech., 20, 349
Vondrák, J. 1977, Bull. Astron. Inst. Czech., 28, 84

Pages 11 to 29 are available in the electronic edition of the journal at http://www.aanda.org

Appendix A: Spectroscopy

Spectroscopic observations at our disposal consist of the following series of electronic spectrograms obtained at Ondřejov and the Dominion Astrophysical Observatory:

1. 23 spectrograms secured in the coude focus of the Ondřejov 2-m telescope and a 702-mm focal length camera with a Reticon 1872RF linear detector. The spectra cover the wavelength region 6300–6730 A with a resolution of 11–12 km s^{-1} per pixel.
2. 239 spectrograms secured with the same spectrograph configuration but with a SITe-005 800 × 2000 CCD detector covering the region 6260–6760 A.

Table A.1. Journal of RVs collected from the literature. For columns "Source" and "Spg. No." the same notation as in Table 1 is used.

HJD −2 400 000	RV [km s^{-1}]	Source	Spg. No.
17 065.8681	−15.6	A	1
18 182.8255	−4.6	A	1
18 287.4889	−9.9	A	1
19 277.8325	−2.3	A	1
19 290.7912	−12.6	A	1
20 744.9629	−13.0	B	2
20 744.9829	12.0	B	2
20 771.9941	19.0	B	2
20 796.8744	3.0	B	2
24 025.9525	−9.3	C	3
24 369.9970	−10.5	C	3
24 418.9749	−11.5	C	3
24 438.8014	−9.5	C	3
24 761.9948	−12.1	C	3
24 767.9082	−11.9	C	3
24 768.9912	−6.7	C	3
41 881.893	−42.5	D	4
41 951.960	−30.1	D	4
41 952.829	−29.0	D	4
41 957.725	−29.5	D	4
41 958.831	−40.6	D	4
42 011.678	−58.5	D	4
42 032.653	−34.2	D	4
42 033.701	−24.0	D	4
42 103.609	−27.1	D	4
42 320.787	−9.8	D	4
42 348.835	−12.4	D	4
42 390.594	7.7	D	4
42 403.683	2.2	D	4
42 404.721	−8.3	D	4
42 424.624	1.7	D	4
42 425.586	6.4	D	4
42 452.610	−18.9	D	4
42 602.963	3.1	D	4
42 650.826	−12.0	D	4
42 724.706	−18.0	D	4
37 274.70	5.8	E	5
37 329.65	−31.6	E	5
37 330.65	−30.4	E	5
37 889.00	−29.2	E	5
43 082.85	−36.3	E	5
43 101.70	−42.8	E	5
22 525.	−80.	F	6
45 980.352	−39.	G	7
45 980.614	−24.	G	7
45 981.479	−48.5	G	7

Table A.2. Hα peak intensities of *o* Cas in the units of the continuum level collected from the literature.

HJD −2 400 000	Peak Int.	Reference
42 762.0	0.71	Slettebak & Reynolds (1978)
43 098.0	1.15	″
43 309.0	1.38	″
43 176.0	1.26	Elias et al. (1978)
43 326.0	1.58	″
43 328.0	1.53	″
43 329.0	1.51	″
44 604.4	1.90	Andrillat & Fehrenbach (1982)
44 895.0	2.20	Barker (1983)
45 155.0	2.42	″
47 533.0	3.88	Slettebak et al. (1992)
47 808.0	4.28	″
51 171.0	6.36	Banerjee et al. (2000)
51 369.60	5.6	Buil (http://www.astrosurf.com/buil)
51 462.40	5.6	″
52 121.6067	3.74	″
52 209.3607	3.98	″
52 260.2756	3.95	″
52 500.5903	4.35	″
52 842.6136	4.73	″
52 907.4497	4.79	″
53 960.5819	5.73	″
54 786.4862	6.33	BeSS (http://basebe.obspm.fr/basebe)
54 700.4843	6.86	″
54 336.5403	5.72	″
55 074.3367	7.16	″
49 559.5695	5.95	″
54 750.4181	6.77	″
54 337.4577	6.34	″
55 059.4836	6.58	″
49 235.5770	4.79	″
54 708.4950	7.64	″
54 354.4642	6.10	″
55 059.4623	6.45	″

Notes. The Hα peak intensities were measured by HB from the publicly available spectra from the C. Buil Castalet Tolosan Observatory and the BeSS database and from the plots of profiles published by Elias et al. (1978), Barker (1983) and Andrillat & Fehrenbach (1982). We adopted the published values from Slettebak & Reynolds (1978), Slettebak et al. (1992) and Banerjee et al. (2000).

3. Two echelle spectrograms secured in the Cassegrain focus of the Ondřejov 2-m telescope with the Heros spectrograph (Kaufer 1988).
4. 178 DAO spectra obtained with the 1.22-m reflector and a CCD detector by SY and in the robotic mode also by PK. These spectra cover the wavelength region 6150–6750 A with a resolution of 6 km s^{-1} per pixel. For further details on the DAO 21181 and 9681 spectrographs, readers are referred to Richardson (1968).

In all cases, calibration arc frames were obtained before and after each stellar frame. During each night, a series of flat field and bias exposures were obtained, usually at the beginning, middle, and the end of the night. These were later averaged for the processing of the stellar data frames. For the 1.8-m data, the exposure times ranged from 15 to 30 min, with S/N between 70 and 150, while for the 1.2 m data exposure times of 20 min were used, giving S/N between 32 and 180.

The initial reduction of Reticon spectra was carried out with the program SPEFO (Horn et al. 1996; Škoda 1996). We used

Table A.3. Individual radial velocities from the Hα emission line wings and He I 6678 absorption line and the peak intensity of the Hα emission.

Time of obs. (HJD-2 400 000)	RV(Hα emis.) [km s^{-1}]	RV(He I 6678 abs.) [km s^{-1}]	Peak int. of Hα emis.	Time of obs. (HJD-2 400 000)	RV(Hα emis.) [km s^{-1}]	RV(He I 6678 abs.) [km s^{-1}]	Peak int. of Hα emis.
Ondřejov Reticon							
48 813.5204	7.40	22.37	4.858	49 660.3695	12.98	15.73	5.405
48 892.3603	−4.05	3.31	–	49 661.2361	12.63	6.55	5.362
49 177.5350	–	−21.75	–	49 915.4553	−3.60	−19.30	5.458
49 212.5177	−28.07	−29.32	–	49 930.4131	−5.42	−5.99	5.609
49 212.5315	−29.10	−31.16	5.157	50 105.2462	−24.23	−22.59	5.749
49 213.4910	–	−36.26	–	50 295.4769	−25.17	−35.63	5.397
49 249.3976	−27.64	−29.80	–	50 365.4353	−21.53	−21.68	5.740
49 594.3943	7.89	11.53	5.366	50 510.2594	−1.64	−4.39	5.762
49 612.3942	10.57	16.26	5.400	51 431.5780	−13.86	−36.44	5.286
49 625.3608	13.83	10.88	–	51 509.3553	−2.78	−12.13	5.216
49 625.4638	11.47	9.64	5.438	51 509.3780	−4.50	−19.56	–
49 659.4048	12.24	8.98	–				
Ondřejov CCD							
52 280.3725	−30.32	−50.70	4.107	52 890.3936	5.25	−0.97	4.734
52 751.6296	9.67	−4.27	4.517	52 890.3990	5.72	0.08	–
52 752.6061	8.91	1.85	4.609	52 890.5053	5.56	−4.69	4.756
52 754.5607	7.75	−0.01	4.563	52 890.5140	4.99	6.84	–
52 754.5728	7.63	3.33	4.592	52 890.6309	5.70	4.64	4.716
52 834.5088	9.08	2.22	4.506	52 890.6380	5.79	−2.18	–
52 834.5147	9.67	–	4.690	52 898.4136	6.93	5.23	4.728
52 835.4675	8.42	8.47	4.702	52 898.4165	6.83	16.06	4.719
52 835.4702	9.21	2.95	4.728	52 898.4190	6.48	5.35	4.737
52 837.4185	8.60	0.34	4.677	52 898.4267	5.49	2.08	–
52 839.4692	7.18	15.01	4.682	52 898.5354	5.75	4.58	4.731
52 839.4712	8.61	−2.54	4.666	52 898.5431	5.46	−6.05	–
52 839.4743	8.13	14.84	4.640	52 901.3950	–	−4.21	–
52 839.5546	8.63	−1.17	4.689	52 901.4048	3.97	3.79	4.717
52 839.5775	8.15	6.41	4.673	52 901.5651	4.79	4.81	4.708
52 839.5813	8.29	11.18	4.674	52 901.6333	4.71	9.34	4.730
52 840.3770	8.46	3.84	4.686	52 903.5120	5.05	14.29	4.742
52 840.3793	8.72	−5.11	4.693	52 903.5180	5.69	5.14	–
52 840.4319	9.64	−1.89	4.712	52 903.6699	5.37	9.86	4.712
52 840.4723	10.25	1.05	4.694	52 903.6720	5.62	3.79	4.724
52 846.4602	8.93	3.99	4.688	52 904.5179	6.36	−6.21	4.768
52 847.5005	10.40	4.10	–	52 904.5219	5.34	0.85	–
52 847.5111	10.64	9.50	–	52 904.5682	5.43	0.35	4.761
52 847.5197	7.90	5.64	–	52 904.6114	5.93	3.75	4.762
52 847.5326	8.04	3.46	4.671	52 905.3573	5.45	2.10	4.725
52 853.5215	–	20.72	–	52 905.3596	6.22	5.82	4.735
52 853.5258	8.57	9.07	4.691	52 905.3643	6.68	2.20	–
52 853.5307	8.15	18.98	–	52 905.4536	4.97	5.27	4.753
52 857.5131	7.96	11.82	4.613	52 905.4577	4.61	4.96	–
52 872.3464	6.51	12.52	4.701	52 905.5145	4.31	4.64	4.722
52 872.3514	6.40	12.42	4.673	52 905.5165	5.25	14.19	4.760
52 872.3637	6.87	15.20	–	52 905.5209	4.64	2.65	–
52 878.3827	8.73	4.64	–	52 909.3454	4.76	2.79	4.763
52 878.3877	5.66	9.09	4.734	52 909.3474	5.24	9.65	4.753
52 878.3947	6.65	4.32	–	52 909.3503	4.85	7.53	4.754
52 878.4002	6.14	−2.51	4.679	52 909.3556	5.36	7.44	–
52 878.4048	6.30	2.83	–	52 909.3654	4.43	10.55	–
52 878.4736	6.71	−8.28	4.709	52 910.3658	4.12	−7.44	4.719
52 878.4805	6.33	11.52	4.718	52 910.3701	4.10	2.34	–
52 878.4863	7.77	2.56	4.696	52 910.5201	5.00	8.19	4.769
52 878.4922	6.15	5.56	4.690	52 910.5244	4.52	3.65	–
52 878.5848	6.80	8.13	4.688	52 932.3227	4.55	2.25	4.776
52 878.5923	6.80	6.41	4.740	52 932.3296	3.35	3.35	4.785
52 878.5988	6.78	−2.83	4.727	52 932.3472	2.81	−0.65	4.789
52 879.4793	6.99	5.80	4.720	52 947.3833	2.00	−4.51	4.743
52 879.4840	7.10	3.60	4.705	52 947.3894	0.70	−9.24	–
52 879.4870	8.72	23.08	4.725	52 947.4687	0.51	−6.36	4.759
52 879.4887	7.05	−0.46	4.718	52 947.4775	−0.09	−12.11	–
52 879.4949	7.17	−2.06	4.708	52 947.6348	−0.37	0.25	4.745
52 879.5107	7.73	0.81	4.722	52 947.6441	0.72	−3.85	4.745

Table A.3. continued.

Time of obs. (HJD-2 400 000)	RV(Hα emis.) [km s^{-1}]	RV(He I 6678 abs.) [km s^{-1}]	Peak int. of Hα emis.	Time of obs. (HJD-2 400 000)	RV(Hα emis.) [km s^{-1}]	RV(He I 6678 abs.) [km s^{-1}]	Peak int. of Hα emis.
52 889.5510	8.23	5.05	4.716	52 952.4429	1.17	3.32	–
52952.4614	1.12	4.13	4.732	53 633.4321	-3.83	-7.22	5.642
52 955.2823	−1.15	−12.21	4.835	53 633.4432	−2.19	−6.74	5.627
52 955.2915	−0.48	−3.47	4.826	53 633.4529	−3.43	0.09	5.644
52 955.3712	−0.71	−14.09	4.848	53 633.4641	−2.79	−8.51	5.631
52 955.4146	0.14	−2.87	4.834	53 633.4740	−2.42	−0.65	5.633
52 955.4855	−1.10	−8.99	4.777	53 633.4848	−3.45	−14.34	5.612
52 955.5943	−0.78	−10.68	4.804	53 633.4959	−4.15	−12.73	5.639
52 955.6499	−0.28	−0.97	4.781	53 637.5807	−1.90	12.72	5.663
52 981.3678	−3.43	−8.86	4.841	53 637.5942	−1.82	14.54	5.650
52 981.3861	−3.88	−7.86	4.831	53 640.2798	−1.11	11.18	5.573
53 224.5475	−31.12	−49.53	5.153	53 640.2942	−0.05	–	5.631
53 224.5505	−30.78	−31.61	5.140	53 650.5013	0.02	6.53	5.640
53 259.4057	−32.25	−11.84	5.186	53 650.5053	−0.93	−0.17	5.608
53 259.4121	−32.74	−27.50	–	53 650.5093	−0.30	3.91	5.623
53 259.4202	−32.86	−26.28	5.165	53 650.5133	−1.78	8.77	5.653
53 259.4279	−32.49	−35.71	5.172	53 658.4761	−0.57	−0.97	5.574
53 259.4359	−33.63	−33.40	5.162	53 658.4810	−1.04	−3.75	5.568
53 259.4450	−33.40	−34.32	5.125	53 658.4849	−1.72	−10.74	5.576
53 259.4550	−32.82	−32.60	5.141	53 658.4887	−2.29	−3.25	5.581
53 259.4646	−33.36	−29.09	5.093	53 658.4925	−2.55	−4.08	5.581
53 259.4742	−34.17	−35.65	5.159	53 658.4962	−1.87	−1.67	5.586
53 259.4839	−33.54	−35.00	5.186	53 658.5002	−0.85	−4.12	5.578
53 259.4936	−33.26	−31.86	5.121	53 658.5039	−0.19	−0.58	5.572
53 264.5495	−33.68	−31.67	5.173	53 745.3950	7.63	0.30	5.546
53 264.5549	−34.88	−32.27	5.177	53 764.3186	7.79	5.15	5.621
53 267.4514	−33.26	−42.38	–	53 764.3317	7.33	−5.10	5.632
53 290.5064	−34.89	–	5.208	53 764.3494	8.60	−6.14	5.614
53 290.5169	−34.03	−33.98	5.152	53 764.3683	7.97	1.87	5.581
53 291.3381	−33.92	−38.99	5.108	53 764.3895	8.40	1.72	5.574
53 303.5426	−33.51	−33.06	5.102	53 764.4183	10.41	7.77	5.573
53 303.5494	−35.09	−31.17	5.122	53 989.6375	−1.41	−5.84	5.728
53 335.4135	−33.45	−30.33	5.135	53 989.6409	1.96	−11.13	5.721
53 335.4220	−33.45	−35.52	5.151	53 990.5045	−1.17	−5.63	5.726
53 335.4851	−33.14	−35.89	5.157	53 990.5089	−1.56	−8.91	5.762
53 335.5581	−33.56	−34.80	5.168	53 990.5138	−0.80	7.98	5.774
53 350.2413	−32.24	−43.37	5.144	53 991.3306	0.42	1.60	5.820
53 360.3863	−31.07	−25.20	5.155	53 991.3337	−1.00	−3.26	5.821
53 360.3999	−33.43	−41.36	5.138	53 991.3366	0.85	13.00	5.799
53 361.2897	−31.91	−29.07	5.175	53 991.3395	−0.34	5.45	5.823
53 361.3255	−31.84	−30.77	5.187	53 991.4219	−0.44	−11.92	5.808
53 377.3186	−30.83	−25.01	5.205	53 991.4248	−0.43	5.95	5.818
53 377.3342	−30.02	−31.13	5.201	53 991.4277	−0.65	−12.33	5.791
53 377.3428	−31.55	−27.46	5.201	53 991.4305	0.06	−2.77	5.800
53 377.3555	−30.38	−30.92	5.196	53 991.4333	−1.43	−5.40	5.806
53 377.3681	−30.89	−19.89	5.204	53 991.6030	−0.16	−7.01	5.783
53 377.3809	−32.03	−23.32	5.190	53 991.6063	−0.13	−17.93	5.765
53 377.3937	−31.20	−31.71	5.200	53 991.6102	−0.63	−13.25	5.793
53 377.4065	−29.75	−27.39	5.200	53 991.6142	−0.96	−5.51	5.801
53 386.4742	−30.99	−40.14	5.189	53 993.3746	−0.33	−3.76	5.790
53 387.2516	−30.06	−26.68	5.201	53 993.3785	−0.57	2.32	5.779
53 394.2466	−29.54	−32.46	5.202	53 993.3825	0.50	−9.00	5.771
53 463.2636	−23.45	−21.83	5.144	53 993.3865	−1.01	−14.83	5.758
53 463.2688	−24.07	−23.58	5.313	53 993.3905	−0.53	−4.52	5.767
53 575.4682	−11.17	−27.21	5.493	53 993.3945	−0.71	−8.75	5.786
53 575.4771	−11.15	−8.74	5.458	53 993.5121	0.32	3.77	5.757
53 612.6044	−4.75	−8.96	5.600	53 993.5160	0.21	9.42	5.729
53 612.6077	−5.48	−3.36	5.601	53 993.5200	0.06	−2.26	5.781
53 612.6111	−5.24	−1.96	5.591	53 993.5240	−0.24	2.04	5.780
53 612.6154	−5.70	−9.35	5.562	53 993.5290	0.47	3.34	5.767
53 612.6175	−4.48	−11.54	5.598	53 993.5757	0.28	3.15	5.752
53 612.6198	−4.77	−4.34	5.558	53 993.5800	0.25	−4.37	5.774
53 613.5923	−4.01	−11.72	5.574	53 993.5853	0.09	12.76	5.757
53 613.5948	−5.64	3.94	5.551	54 116.3661	−17.06	−31.14	6.049
53 613.5972	−4.42	5.74	5.596	54 186.2728	−24.69	−32.13	6.135

Table A.3. continued.

Time of obs. (HJD-2 400 000)	RV(Hα emis.) [km s^{-1}]	RV(He I 6678 abs.) [km s^{-1}]	Peak int. of Hα emis.	Time of obs. (HJD-2 400 000)	RV(Hα emis.) [km s^{-1}]	RV(He I 6678 abs.) [km s^{-1}]	Peak int. of Hα emis.
54 314.5782	−33.98	−29.25	6.036	54 374.6565	−31.51	−26.44	6.027
54 374.6210	−31.17	−24.36	6.035	54 385.4407	−32.98	–	6.007
54 374.6302	−31.21	−26.72	6.013	54 385.4479	−32.71	–	5.976
54 374.6367	−30.95	−25.89	6.023	54 385.4562	−34.81	–	5.994
54 374.6440	−31.26	−26.18	6.027				
DAO CCD							
52 706.6620	7.86	8.59	4.780	53 813.6591	9.93	30.19	5.655
52 771.9888	9.93	8.96	4.726	53 814.6348	9.95	15.54	5.731
52 813.9247	10.41	14.12	4.767	53 909.9306	6.37	9.61	5.715
52 824.9356	10.33	11.21	4.783	53 910.9609	7.43	10.64	5.738
52 825.9496	10.51	13.29	4.796	53 911.9730	8.04	6.78	5.713
52 826.9733	8.30	21.42	4.742	53 912.9853	7.09	23.78	–
52 827.9662	9.68	2.52	4.790	53 948.9079	3.12	4.46	5.744
52 868.9177	7.09	18.55	4.848	53 986.8713	−.5	−8.2	5.857
52 870.0004	8.36	10.28	4.831	53 986.8799	1.1	−15.2	–
52 870.8808	7.61	8.44	4.793	53 986.8911	2.6	−10.7	–
52 872.9699	8.31	11.25	4.717	53 986.9024	.1	−12.5	–
52 872.9786	7.00	8.16	4.793	53 986.9137	.8	7.2	–
52 875.9221	7.05	3.99	4.677	53 986.9250	.9	4.5	–
52 875.9304	8.00	15.21	4.772	53 986.9362	.0	−12.0	–
53 065.6071	−13.57	−3.57	4.892	53 986.9475	.0	.4	–
53 077.6149	−14.23	−20.90	5.020	53 986.9588	.1	−5.0	–
53 079.6815	−14.89	−9.21	5.094	53 986.9701	.3	6.7	–
53 226.9192	−29.26	–	–	53 986.9813	.3	−7.1	–
53 226.9313	−29.36	–	–	53 986.9926	.4	−6.2	5.734
53 226.9389	−30.15	−13.40	–	53 987.0039	.0	−3.0	5.821
53 227.9750	−31.30	−14.57	5.337	53 987.0152	−.3	−3.4	5.776
53 227.9796	−29.62	−24.19	5.255	53 988.7825	1.3	−6.4	–
53 227.9829	−29.98	−31.08	5.188	53 988.7938	.8	−3.3	–
53 229.0076	−29.33	−37.95	5.233	53 988.8051	.0	−1.4	5.817
53 229.9937	−31.82	−30.19	5.326	53 988.8163	−.3	2.0	5.838
53 230.0041	−30.40	–	5.124	53 988.8276	.2	−5.5	5.825
53 231.0189	−30.01	–	–	53 988.8389	−.4	1.8	5.858
53 238.8555	−30.39	−43.10	5.037	53 988.8502	.7	−10.9	–
53 240.7850	−29.60	−14.61	5.181	53 988.8615	.1	−4.3	–
53 240.8330	−31.32	−39.47	5.172	53 988.8727	.2	1.2	–
53 260.7869	−31.21	−32.71	5.205	53 988.8840	.3	−.8	–
53 273.8230	−32.09	−48.17	5.189	53 988.8953	1.1	−4.0	–
53 273.8268	−31.26	−30.51	5.058	53 988.9066	.2	.5	–
53 274.9010	−33.01	−34.76	5.089	53 988.9178	−.3	−9.0	5.774
53 275.9769	−33.30	−47.24	5.079	53 988.9291	−.7	−2.7	5.766
53 275.9811	−32.97	−34.66	5.105	53 990.6697	.0	−5.4	–
53 385.6999	−30.31	−22.05	5.305	53 990.6809	.2	−4.5	–
53 470.0408	−22.37	−28.67	5.132	53 990.6922	−1.0	−1.3	–
53 470.6423	−22.07	−15.90	5.107	53 990.7035	.9	−2.9	–
53 531.9518	−13.26	–	5.574	53 990.7148	−2.4	−1.2	–
53 568.9452	−9.65	4.45	5.481	53 990.7261	−2.0	−4.1	–
53 569.9709	−9.61	−5.04	5.487	53 990.7896	.2	−5.2	–
53 588.0209	−8.21	−17.49	5.411	53 990.8009	.7	−6.7	–
53 588.8953	−7.68	−3.15	5.544	53 990.8122	1.5	−1.2	–
53 589.8887	−6.59	−22.01	5.596	53 990.8235	.7	−3.1	–
53 590.8906	−6.75	−21.66	5.590	53 990.8347	−.2	−3.7	–
53 590.8931	−7.40	−23.38	5.628	53 990.8460	.3	−1.4	–
53 591.9739	−7.69	−5.94	5.631	53 990.8573	.6	−5.8	–
53 636.8884	−2.03	−2.87	5.618	53 990.8686	2.3	−4.5	–
53 637.9865	−1.13	7.15	5.602	53 990.8798	.2	−3.9	–
53 638.9411	−1.04	9.82	5.611	53 990.8911	1.4	−4.7	–
53 639.9290	−0.82	7.38	5.663	53 990.9024	.8	−6.0	–
53 651.6392	0.68	–	5.700	53 990.9137	.5	−1.0	–
53 651.9283	0.20	3.53	5.643	53 990.9250	−.2	−8.0	–
53 654.9946	1.32	−10.45	5.649	53 990.9362	.5	−10.0	–
53 680.9369	1.89	−2.15	5.527	53 991.8082	−1.1	.1	5.797
53 791.6699	8.77	11.26	5.594	54 001.9618	−1.56	6.08	5.831
53 813.6430	11.34	25.33	5.543	54 030.6181	−5.64	-5.11	–

Table A.3. continued.

Time of obs. (HJD-2 400 000)	RV(Hα emis.) [km s^{-1}]	RV(He I 6678 abs.) [km s^{-1}]	Peak int. of Hα emis.	Time of obs. (HJD-2 400 000)	RV(Hα emis.) [km s^{-1}]	RV(He I 6678 abs.) [km s^{-1}]	Peak int. of Hα emis.
54 030.6277	−5.23	−13.21	–	54 032.6479	−4.64	−0.27	–
54 030.6384	−5.96	−8.59	–	54 032.6592	−4.48	6.61	–
54 030.6491	−5.42	4.27	–	54 032.6704	−4.56	6.85	–
54 030.6598	−5.69	−12.33	–	54 032.6817	−4.62	−2.20	–
54 030.6705	−5.92	−14.22	–	54 032.6930	−3.98	−6.96	–
54 030.6812	−5.96	−14.25	–	54 032.7043	−4.32	−1.28	–
54 030.6919	−5.21	2.49	–	54 032.7156	−4.63	−2.89	–
54 030.7026	−6.03	−4.99	–	54 032.7268	−4.32	−2.25	–
54 030.7172	−6.16	3.59	–	54 032.7381	−5.12	−6.71	–
54 030.7285	−5.85	−7.57	–	54 032.7494	−4.59	−6.20	–
54 030.7398	−5.74	5.65	–	54 032.7607	−5.13	−3.09	–
54 030.7510	−5.67	4.99	–	54 032.7719	−4.23	−19.18	5.907
54 030.7623	−6.07	−16.56	–	54 045.0145	−6.22	−21.37	5.856
54 030.7736	−5.81	−11.62	–	54 105.6728	−14.49	−29.32	6.000
54 030.7849	−5.91	−15.21	–	54 106.8467	−14.76	−21.84	6.013
54 030.7962	−5.65	−12.62	–	54 233.0006	−28.67	−41.80	–
54 030.8074	−4.78	16.89	–	54 259.9913	−30.29	−33.83	–
54 030.8187	–	−10.94	–	54 274.8745	−30.52	−25.78	6.193
54 031.7310	−4.40	−11.05	5.914	54 276.9240	−32.89	−30.02	6.130
54 031.7397	−5.00	−14.38	–	54 339.7988	−32.70	−26.02	6.102
54 031.7510	−5.19	−13.89	–	54 340.9310	−32.52	−26.33	6.068
54 031.7623	−4.98	−12.74	–	54 341.9804	−34.37	−34.75	6.148
54 031.7735	−5.04	−11.20	–	54 365.8947	−33.05	−17.53	6.048
54 031.7848	−4.18	−15.01	–	54 367.9798	−32.01	−36.89	6.094
54 031.7961	−5.24	−13.06	–	54 490.7633	−24.73	−28.27	6.160
54 031.8074	−5.38	−16.15	–	54 490.7697	−24.73	−23.72	6.189
54 031.8186	−5.11	−22.18	–	54 491.5740	−22.73	−15.48	6.189
54 031.8299	−5.25	−19.32	–	54 492.7882	−21.78	−21.37	6.158
54 031.8412	−4.96	−19.36	–	54 518.7061	−21.02	−21.09	6.173
54 032.6279	−4.16	−2.72	5.886	54 520.6765	−18.63	−22.23	6.254
54 032.6366	−4.65	−2.34	–	54 598.9940	−10.42	−13.04	6.367
HEROS							
52 695.2924	10.4	5.1	–	52 695.3361	6.9	−3.2	–

the most advanced version JK2.63, which was developed by the late Mr. J. Krpata. The initial reductions of the DAO spectra (bias subtraction, flat fielding and conversion to 1D images) were carried out by SY in IRAF. The initial reduction of the Ondřejov CCD and Heros spectra, which included also the wavelength calibration, was carried out by MŠ, also in IRAF. The final reduction of all spectra (including wavelength calibration for the DAO spectra, continuum rectification and removal of cosmics and flaws) was carried in SPEFO by PK and PH. SPEFO was also used to reduce RV measurements via a comparison of direct and flipped line profiles on the computer screen. Following Horn et al. (1996) we routinely measured a selection of telluric lines and used them to calibrate the wavelength scale of each spectrum. Thanks to that, the spectra from all instruments are on the same heliocentric wavelength scale for all practical purposes.

Appendix B: Photometry

Photometric observations listed in Table 2 were secured at several ground-based observatories and during the Hipparcos mission. Below we provide some comments on the individual sets:

- *Station 1: Hvar* Differential *UBV* observations relative to HR 189 = HD 4142 have continued quite regularly since 1982 (JD 2 445 212.6). The check star HR 289 = HD 6114 was observed as frequently as the the target. Observations secured before the year 2000 (JD 2 451 512.3) have already been analyzed in Pavlovski et al. (1997) and the individual observations were published by Harmanec et al. (1997). Each season of observations was reduced and carefully transformed into the standard *UBV* system with the help of the program HEC22. More recent observations were reduced with rel. 16 of the program which allows also modelling of variable extinction during the observing night. All standard magnitude differences were added to the following *UBV* magnitudes of HR 189

  $V = 5^{\rm m}.674$, $B - V = -0^{\rm m}.127$, $U - B = -0^{\rm m}.566$,

  which were derived from all-sky observations on good nights over many observing seasons.
  The secular constancy of the comparison and check stars as well as the quality of our seasonal transformation to the standard system is documented by the seasonal differential and all-sky *UBV* magnitudes of the check star HR 289 collected in Table B.1.
- *Station 61: Hipparcos satellite* The photometric broadband $H_{\rm p}$ all-sky observations from the deck of the Hipparcos satellite were transformed to the Johnson *V* magnitude via transformation formulæ derived by Harmanec (1998). All observations with error flags larger than 1 were excluded.
- *Station 30: San Pedro Mártir* These all-sky observations were originally secured in the 13-color system. Seven m_{58} measurements from Mitchell & Johnson (1969) and

Table B.1. Seasonal all-sky *UBV* values of the check star HR 289.

Epoch HJD-2 400 000	HJD mean	Number of observations	V	B	U	$B-V$	$U-B$
45 648.2343–46 007.4837	45 956.1050	135	6.473 ± 0.011	6.722 ± 0.010	6.820 ± 0.013	0.250	0.098
46 061.2300–46 339.5874	46 226.3834	42	6.471 ± 0.009	6.721 ± 0.012	6.816 ± 0.019	0.250	0.095
46 436.2196–46 715.5037	46 600.2144	21	6.469 ± 0.011	6.721 ± 0.013	6.815 ± 0.015	0.253	0.093
47 787.4750–47 915.2473	47 828.4701	20	6.476 ± 0.007	6.728 ± 0.010	6.822 ± 0.011	0.252	0.094
49 751.2799–49 751.3633	49 751.3216	2	6.457 ± 0.013	6.712 ± 0.016	6.798 ± 0.007	0.256	0.086
50 863.2342–50 863.3009	50 863.2613	4	6.471 ± 0.017	6.713 ± 0.008	6.804 ± 0.012	0.242	0.091
51 435.5329–51 520.3028	51 476.5423	18	6.475 ± 0.009	6.723 ± 0.011	6.816 ± 0.012	0.248	0.093
51 943.2646–52 284.2443	52 201.4185	29	6.476 ± 0.006	6.723 ± 0.009	6.819 ± 0.008	0.247	0.096
52 544.5069–52 860.6009	52 706.7041	78	6.475 ± 0.007	6.721 ± 0.007	6.817 ± 0.008	0.246	0.096
52 923.4351–53 284.5745	53 174.2352	64	6.474 ± 0.011	6.720 ± 0.011	6.818 ± 0.011	0.246	0.098
53 377.2370–53 686.3523	53 520.6570	29	6.474 ± 0.006	6.722 ± 0.008	6.820 ± 0.011	0.249	0.098
53 744.2360–54 107.2372	53 934.3600	68	6.474 ± 0.008	6.721 ± 0.009	6.818 ± 0.009	0.247	0.096
54 114.3084–54 356.5029	54 175.3724	30	6.472 ± 0.008	6.721 ± 0.008	6.820 ± 0.009	0.249	0.099

Table B.2. All-sky *UBV* photometry of *o* Cas with known times of observations. Note that for observations by Haupt & Schroll (1974) the Julian dates are only known to 1 decimal digit and should not be used for the analysis of rapid variations.

HJD −2 400 000	V	$B-V$	$U-B$	Source
38 295.8415	4.467	−0.065	−0.533	Johnson et al. (1966)
38 298.9317	4.524	−0.059	−0.526	″
38 310.7859	4.518	−0.056	−0.529	″
40 452.6000	4.63	−0.08	−0.52	Haupt & Schroll (1974)
40 458.6000	4.59	−0.07	−0.53	″

Table B.3. Observations in m_{58} band of 13–C photometry.

HJD −2 400 000	m_{58}	Source
39 745.8655	4.589	Mitchell & Johnson (1969)
44 500.9887	4.438	Schuster & Guichard (1984)
44 502.8917	4.465	″
44 503.8665	4.489	″
44 504.8761	4.511	″
44 980.9594	4.450	″
44 892.8040	4.504	″

Schuster & Guichard (1984), derived in the "red system", were adopted to represent the V magnitude without transformation.

– *Station 26: Chiran-OHP* Dates of these 2 all-sky observations were kindly communicated to PH by Dr. H. F. Haupt and are only accurate to about 0.2 d.
– *Station 23: Catalina* These original all-sky *UBV* observations were published by Johnson et al. (1966) and we only derived HJDs from their JDs.

All-sky *UBV* observations compiled from the literature are tabulated in Table B.2, the m_{58} observations in Table B.3, and the Hipparcos H_p observations transformed to Johnson V magnitude are in Table B.4. We derived HJDs of observations in all cases when they were not given in the original sources. All individual *UBV* observations secured since 1982 at Hvar are presented in detail in Table B.5.

Table B.4. Individual all–sky Hipparcos observations of *o* Cas transformed to Johnson *V* magnitudes. Observations with flags larger than 1 were omitted. All times of observations are in HJD-2 400 000.

Time of obs.	*V*	Time of obs.	*V*	Time of obs.	*V*
47 867.7228	4.450	48 219.3769	4.463	48 623.4208	4.487
47 867.7973	4.453	48 219.3912	4.461	48 623.4954	4.493
47 867.8116	4.454	48 219.4657	4.459	48 688.6303	4.481
47 913.4622	4.482	48 219.4800	4.460	48 688.8080	4.477
47 913.4765	4.459	48 219.5546	4.467	48 688.8826	4.486
47 913.5511	4.455	48 219.5689	4.456	48 688.8969	4.491
47 913.5654	4.451	48 219.6435	4.469	48 701.5921	4.484
47 943.4915	4.468	48 219.6578	4.474	48 701.7699	4.499
47 943.5058	4.468	48 219.8213	4.471	48 701.7842	4.503
47 943.6692	4.454	48 219.8356	4.468	48 701.9477	4.494
47 943.6836	4.455	48 219.9102	4.470	48 701.9620	4.485
47 962.3317	4.461	48 219.9245	4.470	48 702.1254	4.490
47 962.3460	4.456	48 219.9990	4.474	48 702.1398	4.477
47 962.4206	4.459	48 220.0134	4.477	48 702.2144	4.482
47 962.4349	4.460	48 220.0879	4.476	48 702.2287	4.484
47 962.5095	4.457	48 220.1023	4.487	48 764.7035	4.492
47 962.5238	4.454	48 259.7937	4.467	48 764.7780	4.489
48 073.8505	4.468	48 259.8081	4.468	48 764.7923	4.492
48 073.8649	4.463	48 259.8826	4.472	48 764.8669	4.486
48 073.9394	4.463	48 282.8060	4.481	48 764.9558	4.487
48 073.9538	4.464	48 282.8203	4.479	48 765.1336	4.485
48 074.0283	4.463	48 308.1285	4.486	48 765.1479	4.484
48 074.0426	4.468	48 308.1428	4.487	48 765.2225	4.485
48 124.9628	4.459	48 308.2174	4.482	48 765.2368	4.479
48 125.0374	4.462	48 308.2317	4.478	48 765.3114	4.480
48 217.7769	4.480	48 418.3209	4.467	48 765.4002	4.476
48 217.8658	4.473	48 418.3352	4.472	48 765.5780	4.493
48 217.8801	4.462	48 418.4098	4.471	48 765.5924	4.489
48 218.0436	4.468	48 418.4241	4.472	48 774.6448	4.493
48 218.0579	4.463	48 440.6430	4.465	48 774.6591	4.488
48 218.1324	4.463	48 440.8954	4.476	48 774.7336	4.488
48 218.1468	4.458	48 440.9097	4.476	48 774.9115	4.492
48 218.2213	4.458	48 470.2193	4.485	48 774.9258	4.492
48 218.2357	4.461	48 470.2336	4.479	48 775.0003	4.492
48 218.3102	4.463	48 470.3225	4.495	48 775.0146	4.486
48 218.3245	4.466	48 506.7342	4.487	48 775.0892	4.491
48 218.4880	4.472	48 506.7485	4.488	48 775.1035	4.486
48 218.5023	4.470	48 517.6670	4.480	48 775.1781	4.487
48 218.5769	4.472	48 517.6813	4.483	48 775.3559	4.487
48 218.5912	4.470	48 517.7559	4.486	48 964.8397	4.492
48 218.6658	4.466	48 517.7702	4.479	48 964.8540	4.491
48 218.6801	4.472	48 606.8034	4.478	48 964.9285	4.490
48 218.9324	4.476	48 606.8780	4.479	48 964.9428	4.487
48 218.9467	4.468	48 606.8923	4.479	49 012.7145	4.468
48 219.0213	4.476	48 606.9669	4.478	49 012.7891	4.490
48 219.0356	4.468	48 606.9812	4.479	49 012.8034	4.493
48 219.1102	4.470	48 623.2430	4.480	49 038.4330	4.490
48 219.1245	4.469	48 623.3176	4.477	49 038.4473	4.485
48 219.1991	4.465	48 623.3319	4.478	–	–
48 219.2134	4.463	48 623.4065	4.480	–	–

Table B.5. Individual differential *UBV* observations of *o* Cas secured at Hvar since 1982 relative to HR 189. We re-publish also the already published part of observations because the all-sky *UBV* values for the comparison star HR 193 have been improved since then. All times of observations are in HJD-2 400 000.

Time of obs.	*V*	*B*	*U*	*B* − *V*	*U* − *B*	*X*	d*X*
Observations by Pavlovski et al. (1997); Harmanec et al. (1997)							
45 212.5601	4.511	4.470	3.870	−.041	−.600	1.006	.001
45 212.5657	4.522	4.476	3.862	−.046	−.614	1.008	.001
45 212.5692	4.511	4.468	3.870	−.043	−.598	1.009	.000
45 216.5326	4.508	4.463	3.863	−.045	−.600	1.004	.001
45 216.5389	4.509	4.465	3.867	−.044	−.598	1.004	.001
45 216.5437	4.518	4.465	3.861	−.053	−.604	1.005	.001
45 217.5299	4.500	4.468	3.863	−.032	−.605	1.004	.001
45 217.5354	4.511	4.471	3.872	−.040	−.599	1.004	.001
45 217.5403	4.529	4.477	3.861	−.052	−.616	1.004	.001
45 219.5099	4.516	4.481	3.878	−.035	−.603	1.007	.001
45 219.5154	4.531	4.482	3.874	−.049	−.608	1.005	.001
45 219.5210	4.515	4.468	3.861	−.047	−.607	1.004	.001
45 224.5282	4.502	4.464	3.864	−.038	−.600	1.006	.001
45 224.5331	4.514	4.467	3.861	−.047	−.606	1.007	.001
45 224.5379	4.513	4.470	3.861	−.043	−.609	1.009	.000
45 225.5956	4.507	4.469	3.864	−.038	−.605	1.076	.000
45 225.5998	4.508	4.474	3.868	−.034	−.606	1.084	.000
45 225.6032	4.520	4.467	3.869	−.053	−.598	1.091	.000
45 226.5936	4.527	4.470	3.874	−.057	−.596	1.077	.000
45 226.5977	4.512	4.484	3.891	−.028	−.593	1.085	.000
45 226.6019	4.520	4.476	3.880	−.044	−.596	1.093	.000
45 227.5846	4.517	4.476	3.864	−.041	−.612	1.067	.000
45 227.5888	4.517	4.501	3.897	−.016	−.604	1.074	.000
45 227.5908	4.509	4.471	3.869	−.038	−.602	1.077	.000
45 231.5834	4.517	4.471	3.864	−.046	−.607	1.083	.000
45 231.5869	4.524	4.473	3.871	−.051	−.602	1.090	.000
45 231.5938	4.509	4.483	3.869	−.026	−.614	1.105	-.001
45 232.5577	4.527	4.488	3.885	−.039	−.603	1.046	.000
45 232.5626	4.524	4.472	3.880	−.052	−.592	1.053	.000
45 239.5115	4.494	4.458	3.853	−.036	−.605	1.018	.000
45 239.5157	4.497	4.451	3.852	−.046	−.599	1.021	.000
45 239.5191	4.498	4.437	3.839	−.061	−.598	1.024	.000
45 269.4072	4.474	4.424	3.850	−.050	−.574	1.006	.001
45 269.4134	4.478	4.425	3.842	−.053	−.583	1.008	.000
45 269.4190	4.468	4.429	3.855	−.039	−.574	1.011	.000
45 307.3631	4.422	4.404	3.821	−.018	−.583	1.062	.000
45 307.3687	4.418	4.408	3.822	−.010	−.586	1.071	.000
45 307.3708	4.423	4.404	3.824	−.019	−.580	1.074	.000
45 308.2658	4.380	4.361	3.781	−.019	−.580	1.007	.001
45 308.2686	4.379	4.367	3.793	−.012	−.574	1.006	.001
45 309.3783	4.307	4.297	3.691	−.010	−.606	1.100	−.001
45 309.3825	4.318	4.299	3.695	−.019	−.604	1.109	−.001
45 309.3845	4.326	4.292	3.695	−.034	−.597	1.113	−.001
45 323.2754	4.463	4.418	3.837	−.045	−.581	1.014	.000
45 323.2796	4.438	4.423	3.839	−.015	−.584	1.017	.000
45 323.2816	4.443	4.418	3.841	−.025	−.577	1.019	.000
45 331.2707	4.451	4.418	3.837	−.033	−.581	1.029	.000
45 331.2756	4.442	4.418	3.834	−.024	−.584	1.034	.000
45 331.2783	4.451	4.412	3.834	−.039	−.578	1.037	.000
45 336.2599	4.461	4.437	3.856	−.024	−.581	1.032	.000
45 336.2634	4.469	4.439	3.850	−.030	−.589	1.036	.000
45 336.2662	4.463	4.433	3.845	−.030	−.588	1.039	.000
45 605.5567	4.464	4.415	3.842	−.049	−.573	1.078	.000
45 605.5608	4.480	4.422	3.840	−.058	−.582	1.085	.000
45 605.5643	4.466	4.428	3.851	−.038	−.577	1.092	.000
45 646.3446	4.424	4.384	3.784	−.040	−.600	1.006	.001
45 646.3480	4.424	4.388	3.790	−.036	−.598	1.005	.001
45 646.3522	4.432	4.393	3.782	−.039	−.611	1.004	.001
45 646.5203	4.406	4.373	3.785	−.033	−.588	1.300	−.003
45 646.5237	4.394	4.377	3.777	−.017	−.600	1.315	−.003
45 646.5258	4.396	4.373	3.780	−.023	−.593	1.325	−.003
45 647.4758	4.456	4.411	3.825	−.045	−.586	1.153	−.001
45 647.4793	4.459	4.419	3.825	−.040	−.594	1.163	−.001

Table B.5. continued. Individual differential *UBV* observations from Hvar.

Time of obs.	*V*	*B*	*U*	*B* − *V*	*U* − *B*	*X*	d*X*
45 647.4820	4.452	4.423	3.831	−.029	−.592	1.171	−.001
45 648.2348	4.417	4.371	3.798	−.046	−.573	1.156	.000
45 648.2404	4.422	4.366	3.795	−.056	−.571	1.141	.000
45 648.2459	4.418	4.370	3.792	−.048	−.578	1.127	.000
45 648.2508	4.401	4.365	3.798	−.036	−.567	1.116	.000
45 648.2563	4.401	4.365	3.797	−.036	−.568	1.103	.000
45 648.2626	4.408	4.369	3.801	−.039	−.568	1.090	.000
45 648.2681	4.417	4.372	3.799	−.045	−.573	1.080	.000
45 648.2737	4.405	4.371	3.797	−.034	−.574	1.070	.000
45 648.2792	4.413	4.368	3.802	−.045	−.566	1.061	.001
45 648.2848	4.423	4.372	3.802	−.051	−.570	1.052	.001
45 648.3022	4.425	4.378	3.806	−.047	−.572	1.031	.001
45 678.2593	4.457	4.426	3.841	−.031	−.585	1.005	.001
45 678.2642	4.452	4.420	3.841	−.032	−.579	1.004	.001
45 683.3354	4.427	4.412	3.820	−.015	−.592	1.065	.000
45 683.3403	4.432	4.408	3.827	−.024	−.581	1.073	.000
45 683.3452	4.432	4.417	3.832	−.015	−.585	1.082	.000
45 689.2330	4.336	4.310	3.729	−.026	−.581	1.004	.001
45 689.2378	4.341	4.314	3.726	−.027	−.588	1.004	.001
45 689.2434	4.345	4.322	3.746	−.023	−.576	1.004	.001
45 698.3115	4.531	4.495	3.937	−.036	−.558	1.099	−.001
45 698.3157	4.531	4.501	3.936	−.030	−.565	1.108	−.001
45 698.3192	4.533	4.499	3.938	−.034	−.561	1.116	−.001
45 699.2642	4.452	4.426	3.830	−.026	−.596	1.030	.000
45 699.2684	4.453	4.421	3.824	−.032	−.597	1.035	.000
45 699.2726	4.447	4.424	3.828	−.023	−.596	1.039	.000
45 706.2186	4.447	4.405	3.839	−.042	−.566	1.010	.000
45 706.2228	4.441	4.397	3.837	−.044	−.560	1.012	.000
45 706.2262	4.445	4.408	3.836	−.037	−.572	1.015	.000
45 711.2231	4.480	4.444	3.865	−.036	−.579	1.023	.000
45 711.2272	4.475	4.441	3.872	−.034	−.569	1.027	.000
45 711.2300	4.476	4.449	3.875	−.027	−.574	1.029	.000
45 712.2424	4.480	4.433	3.843	−.047	−.590	1.048	.000
45 712.2466	4.470	4.422	3.850	−.048	−.572	1.053	.000
45 712.2501	4.459	4.420	3.848	−.039	−.572	1.059	.000
45 713.2521	4.456	4.413	3.832	−.043	−.581	1.066	.000
45 713.2563	4.458	4.413	3.836	−.045	−.577	1.073	.000
45 713.2597	4.451	4.413	3.827	−.038	−.586	1.080	.000
45 918.5383	4.403	4.393	3.795	−.010	−.598	1.057	.001
45 918.5418	4.398	4.372	3.786	−.026	−.586	1.052	.001
45 956.5526	4.413	4.402	3.828	−.011	−.574	1.022	.000
45 956.5574	4.449	4.409	3.827	−.040	−.582	1.026	.000
45 956.5595	4.440	4.406	3.827	−.034	−.579	1.028	.000
45 957.5283	4.429	4.403	3.816	−.026	−.587	1.008	.000
45 957.5325	4.440	4.410	3.830	−.030	−.580	1.010	.000
45 957.5367	4.421	4.399	3.820	−.022	−.579	1.012	.000
45 991.3064	4.421	4.400	3.797	−.021	−.603	1.128	.000
45 991.3106	4.417	4.401	3.800	−.016	−.601	1.118	.000
45 991.3148	4.412	4.387	3.796	−.025	−.591	1.108	.000
45 991.3419	4.422	4.393	3.808	−.029	−.585	1.058	.001
45 991.3453	4.409	4.393	3.799	−.016	−.594	1.053	.001
45 991.3495	4.407	4.385	3.800	−.022	−.585	1.047	.001
45 991.3530	4.406	4.392	3.804	−.014	−.588	1.042	.001
45 991.3564	4.420	4.386	3.798	−.034	−.588	1.038	.001
45 991.3606	4.418	4.393	3.801	−.025	−.592	1.033	.001
45 991.3641	4.410	4.384	3.800	−.026	−.584	1.030	.001
45 991.3676	4.413	4.391	3.799	−.022	−.592	1.026	.001
45 991.3710	4.417	4.389	3.796	−.028	−.593	1.023	.001
45 991.3752	4.411	4.386	3.804	−.025	−.582	1.020	.001
45 991.3828	4.418	4.392	3.798	−.026	−.594	1.014	.001
45 991.3870	4.414	4.390	3.800	−.024	−.590	1.012	.001
45 991.3939	4.415	4.385	3.793	−.030	−.592	1.008	.001
45 991.3995	4.413	4.385	3.801	−.028	−.584	1.006	.001
45 991.4030	4.408	4.381	3.796	−.027	−.585	1.005	.001
45 991.4106	4.415	4.390	3.807	−.025	−.583	1.004	.001

Table B.5. continued.

Time of obs.	V	B	U	$B-V$	$U-B$	X	dX
45 991.4148	4.407	4.385	3.796	−.022	−.589	1.004	.001
45 991.4203	4.415	4.386	3.801	−.029	−.585	1.004	.001
45 991.4245	4.409	4.379	3.792	−.030	−.587	1.005	.001
45 991.4287	4.412	4.391	3.805	−.021	−.586	1.006	.001
45 991.4328	4.412	4.387	3.812	−.025	−.575	1.007	.001
45 991.4370	4.412	4.390	3.811	−.022	−.579	1.008	.000
45 991.4419	4.409	4.382	3.805	−.027	−.577	1.011	.000
45 991.4460	4.410	4.382	3.804	−.028	−.578	1.013	.000
45 991.4537	4.414	4.389	3.809	−.025	−.580	1.018	.000
45 991.4620	4.421	4.393	3.808	−.028	−.585	1.025	.000
45 991.4703	4.415	4.385	3.801	−.030	−.584	1.034	.000
45 991.4773	4.424	4.392	3.807	−.032	−.585	1.042	.000
45 991.4821	4.414	4.393	3.807	−.021	−.586	1.048	.000
45 991.4870	4.419	4.390	3.802	−.029	−.588	1.055	.000
45 991.4905	4.413	4.386	3.807	−.027	−.579	1.061	.000
45 991.5009	4.406	4.379	3.790	−.027	−.589	1.078	.000
45 991.5057	4.413	4.389	3.796	−.024	−.593	1.087	.000
45 991.5113	4.422	4.392	3.809	−.030	−.583	1.099	-.001
45 992.3266	4.424	4.394	3.810	−.030	−.584	1.079	.000
45 992.3315	4.419	4.388	3.805	−.031	−.583	1.070	.000
45 992.3384	4.426	4.394	3.813	−.032	−.581	1.059	.001
45 992.3738	4.415	4.389	3.795	−.026	−.594	1.019	.001
45 992.3773	4.425	4.383	3.802	−.042	−.581	1.016	.001
45 992.3808	4.417	4.389	3.805	−.028	−.584	1.014	.001
45 992.3849	4.412	4.388	3.803	−.024	−.585	1.011	.001
45 992.3884	4.408	4.382	3.793	−.026	−.589	1.010	.001
45 992.3926	4.406	4.374	3.781	−.032	−.593	1.008	.001
45 992.3960	4.412	4.383	3.786	−.029	−.597	1.006	.001
45 992.4044	4.420	4.388	3.800	−.032	−.588	1.004	.001
45 992.4280	4.424	4.400	3.808	−.024	−.592	1.006	.001
45 992.4328	4.413	4.384	3.788	−.029	−.596	1.008	.001
45 992.4363	4.411	4.377	3.788	−.034	−.589	1.009	.000
45 992.4405	4.401	4.375	3.789	−.026	−.586	1.011	.000
45 992.4738	4.410	4.384	3.798	−.026	−.586	1.041	.000
45 992.4808	4.416	4.376	3.786	−.040	−.590	1.050	.000
45 992.4905	4.428	4.377	3.803	−.051	−.574	1.065	.000
45 992.4946	4.411	4.374	3.807	−.037	−.567	1.072	.000
45 992.4988	4.393	4.364	3.797	−.029	−.567	1.079	.000
45 992.5030	4.408	4.369	3.793	−.039	−.576	1.087	.000
45 992.5092	4.407	4.389	3.801	−.018	−.588	1.100	−.001
45 992.5169	4.402	4.365	3.805	−.037	−.560	1.117	−.001
45 992.5238	4.403	4.383	3.804	−.020	−.579	1.134	−.001
45 997.4884	4.382	4.353	3.748	−.029	−.605	1.085	.000
45 997.4933	4.377	4.354	3.753	−.023	−.601	1.095	−.001
45 997.4968	4.376	4.350	3.755	−.026	−.595	1.102	−.001
45 997.5016	4.380	4.351	3.757	−.029	−.594	1.113	−.001
45 997.5058	4.378	4.354	3.760	−.024	−.594	1.123	−.001
46 003.2481	4.417	4.388	3.794	−.029	−.594	1.201	.000
46 003.2558	4.424	4.385	3.806	−.039	−.579	1.177	.000
46 003.2599	4.392	4.370	3.787	−.022	−.583	1.165	.000
46 003.3947	4.411	4.390	3.787	−.021	−.603	1.005	.001
46 003.3988	4.408	4.382	3.782	−.026	−.600	1.006	.001
46 003.4030	4.402	4.392	3.791	−.010	−.601	1.008	.001
46 003.4085	4.408	4.379	3.792	−.029	−.587	1.010	.000
46 003.4127	4.407	4.385	3.795	−.022	−.590	1.013	.000
46 003.4176	4.404	4.382	3.793	−.022	−.589	1.016	.000
46 003.4238	4.408	4.383	3.791	−.025	−.592	1.020	.000
46 003.4280	4.410	4.382	3.796	−.028	−.586	1.024	.000
46 003.4315	4.413	4.381	3.790	−.032	−.591	1.027	.000
46 003.4349	4.410	4.383	3.792	−.027	−.591	1.031	.000
46 003.4412	4.410	4.391	3.795	−.019	−.596	1.038	.000
46 004.4377	4.425	4.388	3.820	−.037	−.568	1.037	.000
46 004.4412	4.424	4.387	3.816	−.037	−.571	1.041	.000
46 004.4446	4.422	4.391	3.810	−.031	−.581	1.046	.000

Table B.5. continued.

Time of obs.	V	B	U	$B-V$	$U-B$	X	dX
46 006.2759	4.414	4.389	3.818	−.025	−.571	1.104	.000
46 006.2807	4.415	4.391	3.800	−.024	−.591	1.094	.000
46 006.2849	4.414	4.398	3.807	−.016	−.591	1.085	.000
46 006.2898	4.419	4.390	3.806	−.029	−.584	1.076	.000
46 006.2939	4.416	4.383	3.805	−.033	−.578	1.069	.000
46 006.2995	4.418	4.388	3.805	−.030	−.583	1.060	.001
46 006.3349	4.414	4.396	3.807	−.018	−.589	1.019	.001
46 006.3398	4.415	4.385	3.796	−.030	−.589	1.015	.001
46 006.3439	4.406	4.383	3.801	−.023	−.582	1.013	.001
46 006.3481	4.417	4.387	3.801	−.030	−.586	1.011	.001
46 006.3523	4.409	4.394	3.796	−.015	−.598	1.009	.001
46 006.3557	4.414	4.388	3.801	−.026	−.587	1.007	.001
46 006.3599	4.416	4.393	3.808	−.023	−.585	1.006	.001
46 006.3682	4.412	4.374	3.799	−.038	−.575	1.004	.001
46 006.3731	4.407	4.382	3.800	−.025	−.582	1.004	.001
46 006.4210	4.419	4.379	3.799	−.040	−.580	1.025	.000
46 006.4259	4.406	4.379	3.798	−.027	−.581	1.030	.000
46 006.4321	4.416	4.370	3.801	−.046	−.569	1.037	.000
46 006.4384	4.415	4.387	3.790	−.028	−.597	1.045	.000
46 006.4432	4.419	4.385	3.805	−.034	−.580	1.051	.000
46 006.4502	4.415	4.380	3.790	−.035	−.590	1.062	.000
46 006.4544	4.413	4.384	3.791	−.029	−.593	1.068	.000
46 006.4585	4.414	4.380	3.791	−.034	−.589	1.076	.000
46 006.4620	4.408	4.381	3.806	−.027	−.575	1.082	.000
46 006.4662	4.411	4.364	3.797	−.047	−.567	1.090	.000
46 007.4245	4.419	4.401	3.811	−.018	−.590	1.031	.000
46 007.4286	4.423	4.394	3.813	−.029	−.581	1.036	.000
46 007.4356	4.419	4.398	3.812	−.021	−.586	1.045	.000
46 007.4398	4.423	4.394	3.808	−.029	−.586	1.050	.000
46 007.4460	4.421	4.390	3.801	−.031	−.589	1.059	.000
46 007.4502	4.426	4.390	3.805	−.036	−.585	1.066	.000
46 007.4543	4.424	4.398	3.812	−.026	−.586	1.073	.000
46 007.4578	4.421	4.395	3.796	−.026	−.599	1.079	.000
46 007.4620	4.434	4.400	3.805	−.034	−.595	1.087	.000
46 007.4668	4.415	4.397	3.796	−.018	−.601	1.097	−.001
46 007.4717	4.413	4.400	3.823	−.013	−.577	1.107	−.001
46 007.4807	4.419	4.389	3.812	−.030	−.577	1.129	−.001
46 007.4856	4.421	4.405	3.815	−.016	−.590	1.141	−.001
46 013.3536	4.432	4.417	3.828	−.015	−.589	1.004	.001
46 013.3577	4.421	4.404	3.819	−.017	−.585	1.004	.001
46 013.3598	4.435	4.416	3.826	−.019	−.590	1.004	.001
46 015.2771	4.452	4.444	3.860	−.008	−.584	1.057	.001
46 015.2813	4.455	4.435	3.847	−.020	−.588	1.050	.001
46 047.2918	4.398	4.356	3.787	−.042	−.569	1.013	.000
46 047.3001	4.396	4.364	3.777	−.032	−.587	1.019	.000
46 047.3119	4.396	4.356	3.779	−.040	−.577	1.029	.000
46 047.3216	4.374	4.372	3.763	−.002	−.609	1.040	.000
46 047.3300	4.390	4.362	3.776	−.028	−.586	1.051	.000
46 047.3459	4.394	4.355	3.784	−.039	−.571	1.077	.000
46 047.3598	4.377	4.336	3.778	−.041	−.558	1.105	−.001
46 047.3737	4.424	4.347	3.767	−.077	−.580	1.138	−.001
46 047.3827	4.400	4.365	3.785	−.035	−.580	1.162	−.001
46 047.3939	4.397	4.377	3.783	−.020	−.594	1.196	−.002
46 061.2360	4.430	4.404	3.813	−.026	−.591	1.006	.001
46 061.2464	4.428	4.414	3.819	−.014	−.595	1.010	.000
46 061.2555	4.443	4.422	3.826	−.021	−.596	1.015	.000
46 074.3017	4.419	4.406	3.801	−.013	−.605	1.147	−.001
46 074.3094	4.421	4.417	3.819	−.004	−.598	1.169	−.001
46 077.2182	4.433	4.411	3.816	−.022	−.595	1.020	.000
46 077.2258	4.422	4.403	3.800	−.019	−.603	1.027	.000
46 077.2321	4.429	4.403	3.802	−.026	−.601	1.034	.000
46 077.2383	4.433	4.409	3.819	−.024	−.590	1.041	.000
46 077.2452	4.421	4.412	3.818	−.009	−.594	1.050	.000
46 077.2522	4.426	4.419	3.818	−.007	−.601	1.061	.000

Table B.5. continued.

Time of obs.	V	B	U	$B-V$	$U-B$	X	dX
46 077.2793	4.425	4.399	3.815	−.026	−.584	1.112	−.001
46 078.2257	4.425	4.393	3.810	−.032	−.583	1.030	.000
46 078.2334	4.422	4.392	3.811	−.030	−.581	1.039	.000
46 078.2403	4.420	4.393	3.810	−.027	−.583	1.047	.000
46 094.2321	4.384	4.357	3.758	−.027	−.599	1.114	−.001
46 094.2384	4.389	4.369	3.767	−.020	−.602	1.129	−.001
46 094.2467	4.385	4.370	3.796	−.015	−.574	1.150	−.001
46 094.2557	4.386	4.373	3.768	−.013	−.605	1.176	−.001
46 095.2293	4.441	4.418	3.830	−.023	−.588	1.114	−.001
46 095.2341	4.441	4.425	3.833	−.016	−.592	1.125	−.001
46 095.2404	4.442	4.421	3.826	−.021	−.595	1.141	−.001
46 101.2288	4.433	4.420	3.835	−.013	−.585	1.155	−.001
46 101.2323	4.451	4.408	3.828	−.043	−.580	1.165	−.001
46 101.2344	4.456	4.414	3.833	−.042	−.581	1.171	−.001
46 319.5282	4.399	4.369	3.781	−.030	−.588	1.005	.001
46 319.5344	4.392	4.370	3.783	−.022	−.587	1.007	.001
46 319.5407	4.398	4.377	3.783	−.021	−.594	1.010	.000
46 320.5199	4.437	4.411	3.835	−.026	−.576	1.004	.001
46 320.5261	4.436	4.415	3.833	−.021	−.582	1.005	.001
46 320.5331	4.440	4.416	3.837	−.024	−.579	1.008	.001
46 323.5311	4.447	4.409	3.829	−.038	−.580	1.010	.000
46 323.5388	4.434	4.404	3.830	−.030	−.574	1.015	.000
46 323.5471	4.430	4.405	3.835	−.025	−.570	1.021	.000
46 324.5451	4.452	4.427	3.843	−.025	−.584	1.022	.000
46 324.5520	4.457	4.418	3.836	−.039	−.582	1.028	.000
46 324.5590	4.453	4.418	3.831	−.035	−.587	1.035	.000
46 338.5102	4.435	4.407	3.831	−.028	−.576	1.024	.000
46 338.5192	4.425	4.409	3.826	−.016	−.583	1.033	.000
46 338.5283	4.451	4.415	3.832	−.036	−.583	1.044	.000
46 339.5596	4.434	4.413	3.809	−.021	−.604	1.102	−.001
46 339.5707	4.426	4.400	3.810	−.026	−.590	1.127	−.001
46 339.5825	4.423	4.408	3.815	−.015	−.593	1.158	−.001
46 427.2353	4.464	4.429	3.846	−.035	−.583	1.006	.001
46 427.2429	4.465	4.414	3.834	−.051	−.580	1.009	.000
46 427.2512	4.448	4.421	3.838	−.027	−.583	1.013	.000
46 436.2249	4.383	4.351	3.767	−.032	−.584	1.013	.000
46 436.2339	4.409	4.384	3.786	−.025	−.598	1.019	.000
46 436.2784	4.422	4.388	3.778	−.034	−.610	1.075	.000
46 436.2860	4.420	4.387	3.802	−.033	−.585	1.089	.000
46 436.2957	4.427	4.397	3.809	−.030	−.588	1.110	−.001
46 438.2268	4.473	4.451	3.887	−.022	−.564	1.018	.000
46 438.2317	4.475	4.447	3.885	−.028	−.562	1.022	.000
46 438.2372	4.483	4.460	3.894	−.023	−.566	1.027	.000
46 680.5508	4.388	4.364	3.787	−.024	−.577	1.009	.000
46 680.5557	4.379	4.346	3.775	−.033	−.571	1.012	.000
46 680.5606	4.383	4.348	3.772	−.035	−.576	1.015	.000
46 689.5076	4.395	4.379	3.795	−.016	−.584	1.004	.001
46 689.5138	4.409	4.386	3.804	−.023	−.582	1.005	.001
46 689.5180	4.407	4.382	3.795	−.025	−.587	1.006	.001
46 690.5666	4.424	4.393	3.796	−.031	−.597	1.048	.000
46 690.5736	4.417	4.398	3.807	−.019	−.591	1.057	.000
46 690.5833	4.411	4.391	3.807	−.020	−.584	1.073	.000
46 690.5972	4.415	4.397	3.800	−.018	−.597	1.100	−.001
46 694.5647	4.365	4.331	3.758	−.034	−.573	1.060	.000
46 694.5751	4.361	4.325	3.760	−.036	−.565	1.078	.000
46 694.5842	4.366	4.333	3.762	−.033	−.571	1.095	−.001
46 694.5911	4.358	4.322	3.749	−.036	−.573	1.110	−.001
46 696.5565	4.450	4.422	3.846	−.028	−.576	1.056	.000
46 696.5683	4.453	4.427	3.831	−.026	−.596	1.075	.000
46 696.5738	4.443	4.428	3.828	−.015	−.600	1.086	.000
46 696.5815	4.431	4.419	3.811	−.012	−.608	1.101	−.001
46 705.5096	4.405	4.383	3.809	−.022	−.574	1.028	.000
46 705.5151	4.430	4.402	3.817	−.028	−.585	1.034	.000
46 705.5235	4.413	4.385	3.811	−.028	−.574	1.044	.000

Table B.5. continued.

Time of obs.	*V*	*B*	*U*	*B* − *V*	*U* − *B*	*X*	d*X*
46 715.4966	4.418	4.393	3.804	−.025	−.589	1.044	.000
46 715.4994	4.419	4.400	3.811	−.019	−.589	1.048	.000
46 715.5022	4.426	4.401	3.815	−.025	−.586	1.052	.000
47 787.4820	4.454	4.430	3.827	−.024	−.603	1.006	.001
47 787.4910	4.451	4.429	3.828	−.022	−.601	1.004	.001
47 787.5000	4.448	4.430	3.831	−.018	−.599	1.004	.001
47 788.4598	4.451	4.428	3.830	−.023	−.598	1.016	.001
47 788.4688	4.455	4.423	3.823	−.032	−.600	1.010	.001
47 788.4778	4.456	4.424	3.824	−.032	−.600	1.007	.001
47 791.4544	4.454	4.424	3.815	−.030	−.609	1.014	.001
47 791.4627	4.451	4.424	3.820	−.027	−.604	1.009	.001
47 791.4710	4.453	4.428	3.829	−.025	−.599	1.006	.001
47 900.1851	4.452	4.409	3.817	−.043	−.592	1.004	.001
47 900.1934	4.458	4.411	3.809	−.047	−.602	1.004	.001
47 900.2011	4.465	4.416	3.810	−.049	−.606	1.006	.001
47 907.2186	4.458	4.420	3.825	−.038	−.595	1.031	.000
47 907.2276	4.458	4.418	3.818	−.040	−.600	1.041	.000
47 907.2359	4.460	4.417	3.813	−.043	−.604	1.052	.000
47 911.2141	4.455	4.414	3.819	−.041	−.595	1.038	.000
47 911.2238	4.446	4.408	3.812	−.038	−.596	1.051	.000
47 915.2277	4.456	4.423	3.828	−.033	−.595	1.075	.000
47 915.2367	4.449	4.419	3.821	−.030	−.598	1.092	.000
47 915.2450	4.458	4.419	3.821	−.039	−.598	1.109	−.001
So far unpublished Hvar observations							
49 747.2766	4.507	4.436	3.845	−.071	−.592	1.251	-.002
49 747.2842	4.519	4.444	3.858	−.075	−.586	1.282	-.003
49 747.2919	4.519	4.449	3.870	−.070	−.579	1.315	-.003
50 863.2417	4.542	4.488	3.937	−.054	−.551	1.346	-.004
50 863.2529	4.537	4.494	3.911	−.043	−.583	1.403	-.005
50 863.2619	4.543	4.491	3.916	−.052	−.575	1.455	-.005
51 428.5298	4.542	4.494	3.933	−.047	−.561	1.004	.001
51 428.5396	4.544	4.493	3.920	−.050	−.573	1.005	.001
51 428.5461	4.520	4.486	3.907	−.034	−.579	1.007	.001
51 435.5384	4.473	4.448	3.854	−.025	−.594	1.012	.000
51 435.5451	4.496	4.456	3.868	−.041	−.588	1.016	.000
51 435.5517	4.484	4.454	3.861	−.030	−.594	1.021	.000
51 445.5296	4.516	4.479	3.878	−.037	−.600	1.026	.000
51 445.5361	4.525	4.478	3.880	−.048	−.598	1.032	.000
51 445.5434	4.527	4.477	3.876	−.050	−.601	1.041	.000
51 512.3231	4.564	4.505	3.913	−.058	−.593	1.009	.000
51 512.3307	4.549	4.498	3.894	−.051	−.604	1.013	.000
51 512.3384	4.551	4.495	3.897	−.055	−.599	1.019	.000
51 943.2686	4.451	4.424	3.852	−.027	−.572	1.269	−.003
51 943.2762	4.444	4.423	3.833	−.022	−.590	1.301	−.003
51 943.2845	4.458	4.423	3.833	−.035	−.590	1.340	−.004
52 194.4785	4.391	4.401	3.861	.009	−.540	1.025	.000
52 195.4777	4.359	4.334	3.796	−.024	−.538	1.026	.000
52 195.4838	4.348	4.332	3.802	−.016	−.530	1.033	.000
52 195.4900	4.355	4.326	3.791	−.029	−.534	1.040	.000
52 197.4223	4.386	4.370	3.836	−.015	−.535	1.004	.001
52 197.4290	4.386	4.370	3.837	−.017	−.533	1.004	.001
52 197.4360	4.383	4.370	3.835	−.013	−.535	1.005	.001
52 208.4492	4.391	4.361	3.836	−.030	−.525	1.033	.000
52 208.4581	4.401	4.370	3.855	−.031	−.515	1.044	.000
52 208.4659	4.392	4.368	3.847	−.024	−.521	1.055	.000
52 208.4685	4.397	4.357	3.848	−.039	−.509	1.059	.000
52 211.4136	4.365	4.355	3.816	−.010	−.539	1.011	.000
52 211.4226	4.366	4.354	3.813	−.013	−.541	1.017	.000
52 211.4288	4.362	4.348	3.807	−.014	−.541	1.022	.000
52 245.4334	4.362	4.329	3.791	−.033	−.538	1.223	−.002
52 245.4473	4.362	4.334	3.774	−.028	−.560	1.276	−.003
52 245.4604	4.355	4.325	3.804	−.030	−.521	1.334	−.003
52 246.4687	4.362	4.352	3.801	−.010	−.551	1.389	−.004
52 246.4847	4.380	4.351	3.816	−.029	−.535	1.482	−.006
52 246.4972	4.381	4.364	3.831	−.017	−.533	1.566	−.007

Table B.5. continued.

Time of obs.	V	B	U	$B-V$	$U-B$	X	dX
52 247.4076	4.376	4.353	3.814	−.024	−.539	1.159	−.001
52 247.4187	4.377	4.356	3.822	−.021	−.534	1.192	−.002
52 247.4298	4.382	4.354	3.814	−.029	−.539	1.230	−.002
52 248.2909	4.399	4.355	3.818	−.044	−.537	1.004	.001
52 248.3020	4.391	4.368	3.841	−.023	−.527	1.007	.001
52 252.4198	4.385	4.350	3.816	−.036	−.534	1.244	−.002
52 252.4281	4.380	4.352	3.817	−.028	−.535	1.277	−.003
52 252.4372	4.393	4.368	3.831	−.025	−.537	1.316	−.003
52 263.4421	4.369	4.328	3.796	−.041	−.532	1.513	−.006
52 263.4504	4.372	4.343	3.819	−.029	−.524	1.570	−.007
52 263.4587	4.367	4.328	3.778	−.038	−.550	1.634	−.008
52 276.3460	4.389	4.355	3.827	−.034	−.528	1.220	−.002
52 276.3523	4.384	4.355	3.823	−.029	−.533	1.243	−.002
52 276.3571	4.389	4.353	3.823	−.036	−.530	1.261	−.002
52 284.2267	4.357	4.325	3.792	−.032	−.533	1.022	.000
52 284.2336	4.356	4.329	3.795	−.026	−.534	1.029	.000
52 284.2427	4.356	4.326	3.798	−.030	−.528	1.039	.000
52 544.5122	4.389	4.355	3.788	−.035	−.566	1.018	.000
52 544.5179	4.392	4.351	3.785	−.042	−.566	1.023	.000
52 544.5238	4.386	4.354	3.781	−.032	−.573	1.028	.000
52 545.5115	4.398	4.361	3.800	−.037	−.562	1.020	.000
52 545.5169	4.394	4.369	3.807	−.025	−.563	1.024	.000
52 545.5222	4.389	4.370	3.809	−.019	−.561	1.030	.000
52 546.5613	4.371	4.372	3.799	.001	−.573	1.092	.000
52 546.5678	4.391	4.359	3.793	−.033	−.565	1.106	−.001
52 546.5741	4.380	4.357	3.803	−.023	−.554	1.120	−.001
52 549.5111	4.426	4.401	3.845	−.025	−.556	1.029	.000
52 549.5165	4.418	4.390	3.829	−.028	−.561	1.035	.000
52 549.5222	4.421	4.397	3.841	−.024	−.556	1.042	.000
52 561.4845	4.398	4.365	3.815	−.033	−.550	1.036	.000
52 561.4898	4.403	4.370	3.813	−.032	−.558	1.042	.000
52 561.4951	4.407	4.366	3.815	−.042	−.551	1.049	.000
52 584.5134	4.424	4.388	3.822	−.036	−.566	1.250	−.002
52 638.3081	4.402	4.393	3.823	−.009	−.570	1.092	.000
52 638.3157	4.403	4.392	3.825	−.011	−.567	1.109	−.001
52 638.3268	4.416	4.392	3.824	−.024	−.568	1.135	−.001
52 655.2387	4.427	4.413	3.841	−.014	−.571	1.055	.000
52 655.2471	4.424	4.418	3.843	−.006	−.575	1.068	.000
52 655.2554	4.432	4.414	3.843	−.018	−.571	1.083	.000
52 659.2815	4.430	4.405	3.855	−.025	−.551	1.172	−.001
52 659.2919	4.429	4.391	3.842	−.038	−.549	1.205	−.002
52 659.2982	4.438	4.405	3.822	−.033	−.583	1.227	−.002
52 666.2969	4.421	4.423	3.846	.001	−.576	1.300	−.003
52 666.3046	4.425	4.411	3.837	−.014	−.575	1.334	−.003
52 667.2920	4.427	4.404	3.828	−.023	−.576	1.290	−.003
52 667.3010	4.425	4.394	3.821	−.031	−.574	1.331	−.003
52 835.5408	4.430	4.412	3.809	−.018	−.603	1.190	.000
52 835.5478	4.432	4.420	3.815	−.012	−.605	1.169	.000
52 835.5547	4.420	4.414	3.819	−.006	−.595	1.149	.000
52 847.5667	4.434	4.426	3.819	−.008	−.607	1.058	.001
52 847.5737	4.431	4.426	3.824	−.005	−.602	1.048	.001
52 847.5813	4.431	4.431	3.825	.000	−.606	1.038	.001
52 856.5987	4.426	4.408	3.805	−.018	−.603	1.007	.001
52 856.6105	4.445	4.420	3.820	−.025	−.600	1.004	.001
52 857.5592	4.428	4.429	3.837	.001	−.592	1.033	.001
52 857.5689	4.443	4.426	3.824	−.017	−.601	1.023	.001
52 857.5814	4.440	4.422	3.824	−.019	−.598	1.014	.001
52 859.5072	4.418	4.400	3.809	−.019	−.590	1.109	.000
52 859.5156	4.422	4.411	3.804	−.011	−.606	1.092	.000
52 859.5274	4.435	4.414	3.808	−.022	−.606	1.070	.000
52 860.5601	4.434	4.408	3.808	−.027	−.599	1.024	.001
52 860.5677	4.435	4.417	3.810	−.018	−.607	1.018	.001
52 860.5767	4.427	4.416	3.814	−.011	−.602	1.012	.001
52 860.5899	4.433	4.418	3.824	−.015	−.594	1.006	.001

Table B.5. continued.

Time of obs.	V	B	U	$B-V$	$U-B$	X	dX
52 860.5941	4.433	4.413	3.818	−.020	−.594	1.005	.001
52 860.5990	4.426	4.414	3.813	−.013	−.601	1.004	.001
52 869.5357	4.437	4.412	3.822	−.024	−.591	1.025	.001
52 869.5434	4.441	4.422	3.823	−.019	−.599	1.018	.001
52 869.5524	4.430	4.419	3.821	−.011	−.599	1.012	.001
52 923.4409	4.441	4.426	3.827	−.015	−.599	1.004	.001
52 923.4484	4.437	4.424	3.826	−.013	−.599	1.005	.001
52 923.4560	4.435	4.422	3.827	−.013	−.595	1.008	.001
52 929.5139	4.453	4.443	3.831	−.010	−.612	1.093	.000
52 929.5225	4.443	4.431	3.829	−.012	−.602	1.112	−.001
52 929.5294	4.450	4.433	3.837	−.017	−.596	1.128	−.001
52 940.4046	4.452	4.436	3.839	−.015	−.598	1.006	.001
52 946.3778	4.438	4.424	3.826	−.014	−.597	1.004	.001
52 946.3845	4.443	4.421	3.822	−.022	−.599	1.005	.001
52 946.3912	4.441	4.424	3.824	−.017	−.601	1.007	.001
53 028.2806	4.443	4.439	3.832	−.004	−.608	1.202	−.002
53 028.2896	4.454	4.443	3.826	−.011	−.617	1.234	−.002
53 028.2999	4.451	4.434	3.815	−.018	−.619	1.274	−.003
53 029.3364	4.454	4.429	3.822	−.025	−.608	1.473	−.006
53 035.2509	4.448	4.430	3.835	−.018	−.594	1.171	−.001
53 035.2589	4.448	4.434	3.830	−.013	−.604	1.196	−.002
53 035.2656	4.453	4.428	3.826	−.025	−.602	1.218	−.002
53 232.5486	4.463	4.438	3.830	−.026	−.608	1.019	.001
53 232.5565	4.471	4.443	3.831	−.028	−.612	1.013	.001
53 232.5645	4.458	4.438	3.830	−.020	−.608	1.009	.001
53 235.5386	4.452	4.428	3.817	−.024	−.611	1.020	.001
53 235.5464	4.457	4.431	3.824	−.026	−.607	1.015	.001
53 235.5575	4.462	4.436	3.823	−.026	−.613	1.009	.001
53 236.5722	4.449	4.425	3.821	−.024	−.604	1.004	.001
53 236.5783	4.453	4.428	3.817	−.025	−.611	1.004	.001
53 236.5845	4.459	4.428	3.818	−.031	−.610	1.005	.001
53 238.5183	4.461	4.441	3.830	−.021	−.610	1.032	.001
53 238.5261	4.459	4.439	3.831	−.020	−.608	1.024	.001
53 238.5358	4.455	4.439	3.833	−.016	−.606	1.017	.001
53 240.5383	4.456	4.425	3.812	−.031	−.613	1.012	.001
53 240.5456	4.458	4.429	3.816	−.028	−.614	1.008	.001
53 240.5517	4.454	4.426	3.820	−.028	−.606	1.006	.001
53 241.5325	4.458	4.435	3.825	−.023	−.610	1.013	.001
53 241.5402	4.459	4.431	3.824	−.029	−.606	1.009	.001
53 241.5489	4.458	4.432	3.824	−.026	−.608	1.006	.001
53 242.5125	4.470	4.446	3.830	−.024	−.617	1.027	.001
53 242.5186	4.469	4.440	3.826	−.029	−.614	1.022	.001
53 242.5247	4.464	4.443	3.833	−.022	−.610	1.017	.001
53 255.4742	4.455	4.435	3.822	−.020	−.613	1.031	.001
53 255.4794	4.458	4.436	3.825	−.021	−.611	1.026	.001
53 255.4820	4.460	4.438	3.828	−.022	−.610	1.023	.001
53 269.4733	4.482	4.458	3.862	−.024	−.596	1.006	.001
53 277.4789	4.467	4.444	3.834	−.022	−.610	1.005	.001
53 277.4856	4.468	4.441	3.835	−.027	−.606	1.007	.001
53 277.4926	4.459	4.429	3.823	−.029	−.607	1.010	.000
53 278.4384	4.462	4.437	3.825	−.026	−.611	1.011	.001
53 278.4464	4.461	4.435	3.832	−.026	−.603	1.007	.001
53 278.4544	4.460	4.434	3.830	−.027	−.603	1.005	.001
53 279.4389	4.462	4.438	3.830	−.024	−.608	1.009	.001
53 279.4467	4.460	4.433	3.827	−.027	−.606	1.006	.001
53 279.4546	4.453	4.433	3.823	−.020	−.610	1.004	.001
53 376.2511	4.460	4.447	3.811	−.013	−.637	1.036	.000
53 376.2587	4.453	4.431	3.822	−.022	−.610	1.045	.000
53 377.2421	4.464	4.440	3.832	−.024	−.608	1.029	.000
53 377.2495	4.464	4.449	3.835	−.016	−.613	1.037	.000
53 377.2580	4.463	4.447	3.836	−.016	−.612	1.048	.000
53 379.2769	4.465	4.445	3.840	−.020	−.605	1.089	.000
53 379.2817	4.470	4.446	3.841	−.023	−.605	1.099	−.001
53 379.2868	4.472	4.447	3.841	−.024	−.606	1.110	−.001

Table B.5. continued.

Time of obs.	V	B	U	$B-V$	$U-B$	X	dX
53 382.2627	4.470	4.426	3.818	−.044	−.608	1.078	.000
53 382.2662	4.478	4.460	3.866	−.018	−.594	1.084	.000
53 382.2686	4.454	4.433	3.819	−.021	−.615	1.089	.000
53 385.2295	4.462	4.434	3.829	−.028	−.605	1.040	.000
53 385.2358	4.450	4.436	3.822	−.014	−.614	1.049	.000
53 385.2423	4.454	4.433	3.818	−.020	−.615	1.058	.000
53 387.2514	4.476	4.441	3.855	−.035	−.585	1.083	.000
53 387.2611	4.476	4.431	3.830	−.045	−.601	1.102	−.001
53 387.2712	4.463	4.435	3.841	−.028	−.594	1.126	−.001
53 388.2463	4.471	4.439	3.830	−.032	−.609	1.079	.000
53 388.2540	4.476	4.443	3.839	−.034	−.603	1.094	.000
53 388.2605	4.473	4.448	3.839	−.024	−.609	1.107	−.001
53 602.5077	4.485	4.448	3.826	−.036	−.622	1.049	.001
53 602.5190	4.460	4.433	3.819	−.027	−.614	1.035	.001
53 602.5301	4.464	4.430	3.818	−.034	−.612	1.024	.001
53 655.3995	4.470	4.427	3.822	−.043	−.605	1.015	.001
53 655.4092	4.478	4.448	3.839	−.030	−.609	1.009	.001
53 655.4210	4.481	4.435	3.821	−.046	−.615	1.005	.001
53 658.4377	4.473	4.436	3.835	−.037	−.602	1.006	.001
53 658.4474	4.489	4.452	3.856	−.037	−.596	1.009	.001
53 660.3884	4.489	4.444	3.838	−.045	−.606	1.013	.001
53 660.3968	4.479	4.435	3.834	−.044	−.602	1.009	.001
53 660.4044	4.483	4.436	3.829	−.046	−.607	1.006	.001
53 661.3926	4.478	4.438	3.834	−.040	−.604	1.010	.001
53 661.4002	4.481	4.442	3.833	−.039	−.609	1.007	.001
53 661.4093	4.475	4.434	3.826	−.042	−.608	1.004	.001
53 662.4141	4.483	4.439	3.839	−.044	−.600	1.004	.001
53 662.4211	4.486	4.451	3.845	−.035	−.606	1.005	.001
53 662.4301	4.486	4.452	3.846	−.034	−.606	1.007	.001
53 675.4107	4.487	4.452	3.839	−.035	−.613	1.014	.000
53 675.4197	4.462	4.416	3.811	−.046	−.606	1.021	.000
53 675.4287	4.479	4.441	3.838	−.038	−.603	1.029	.000
53 686.3355	4.474	4.438	3.830	−.036	−.607	1.006	.001
53 686.3431	4.484	4.436	3.835	−.048	−.601	1.004	.001
53 686.3508	4.483	4.435	3.828	−.047	−.607	1.004	.001
53 694.3339	4.474	4.433	3.823	−.040	−.610	1.005	.001
53 694.3408	4.470	4.420	3.822	−.049	−.598	1.006	.001
53 694.3498	4.476	4.438	3.827	−.038	−.611	1.010	.000
53 744.2427	4.498	4.460	3.846	−.038	−.615	1.035	.000
53 744.2511	4.494	4.459	3.847	−.035	−.612	1.045	.000
53 744.2622	4.495	4.461	3.847	−.033	−.614	1.062	.000
53 745.2364	4.485	4.460	3.841	−.025	−.620	1.031	.000
53 745.2434	4.482	4.446	3.836	−.036	−.609	1.039	.000
53 745.2531	4.486	4.447	3.838	−.040	−.609	1.052	.000
53 747.2342	4.470	4.433	3.822	−.037	−.611	1.035	.000
53 747.2418	4.469	4.433	3.821	−.036	−.611	1.044	.000
53 747.2508	4.478	4.439	3.828	−.039	−.611	1.057	.000
53 750.2701	4.482	4.449	3.847	−.033	−.603	1.108	−.001
53 750.2819	4.486	4.441	3.839	−.045	−.602	1.136	−.001
53 750.2923	4.472	4.434	3.826	−.038	−.607	1.165	−.001
53 756.2488	4.481	4.443	3.838	−.038	−.605	1.099	−.001
53 756.2578	4.486	4.445	3.832	−.041	−.614	1.119	−.001
53 756.2668	4.477	4.441	3.830	−.036	−.611	1.141	−.001
53 761.2407	4.484	4.447	3.839	−.037	−.608	1.112	−.001
53 761.2477	4.477	4.437	3.821	−.040	−.616	1.128	−.001
53 761.2546	4.485	4.441	3.830	−.044	−.611	1.146	−.001
53 933.5762	4.485	4.429	3.818	−.056	−.611	1.086	.000
53 933.5850	4.478	4.423	3.823	−.055	−.599	1.070	.000
53 933.5942	4.478	4.419	3.811	−.058	−.608	1.055	.001
53 969.5654	4.494	4.455	3.847	−.039	−.608	1.004	.001
53 969.5775	4.496	4.457	3.850	−.039	−.607	1.004	.001
53 969.5896	4.517	4.469	3.850	−.048	−.620	1.008	.001
53 970.5145	4.519	4.481	3.884	−.037	−.597	1.032	.001
53 971.5403	4.492	4.464	3.854	−.028	−.610	1.010	.001

Table B.5. continued.

Time of obs.	V	B	U	$B-V$	$U-B$	X	dX
53 971.5507	4.502	4.479	3.878	−.023	−.601	1.006	.001
53 971.5527	4.517	4.493	3.884	−.024	−.609	1.005	.001
53 978.5025	4.481	4.430	3.811	−.051	−.619	1.023	.001
53 978.5131	4.503	4.461	3.847	−.043	−.613	1.015	.001
53 978.5235	4.480	4.434	3.825	−.046	−.610	1.009	.001
53 979.5342	4.507	4.467	3.848	−.040	−.619	1.005	.001
53 979.5469	4.503	4.465	3.859	−.038	−.606	1.004	.001
53 979.5592	4.487	4.452	3.852	−.035	−.601	1.006	.001
53 980.5111	4.510	4.450	3.843	−.060	−.607	1.013	.001
53 980.5215	4.484	4.437	3.832	−.047	−.605	1.008	.001
53 980.5313	4.484	4.443	3.834	−.041	−.609	1.005	.001
53 981.5147	4.495	4.431	3.816	−.064	−.615	1.009	.001
53 981.5268	4.504	4.454	3.846	−.050	−.608	1.005	.001
53 983.4090	4.489	4.434	3.821	−.055	−.613	1.169	.000
53 983.4168	4.480	4.452	3.842	−.027	−.610	1.147	.000
53 983.4249	4.505	4.468	3.852	−.037	−.616	1.126	.000
53 984.4741	4.501	4.475	3.878	−.026	−.597	1.035	.001
53 984.4849	4.492	4.481	3.893	−.011	−.588	1.024	.001
53 984.4999	4.489	4.450	3.803	−.039	−.646	1.013	.001
53 989.5129	4.505	4.481	3.855	−.024	−.625	1.004	.001
53 989.5232	4.500	4.476	3.861	−.024	−.614	1.004	.001
53 989.5336	4.490	4.459	3.831	−.031	−.628	1.007	.001
53 999.4434	4.482	4.436	3.822	−.047	−.613	1.025	.001
53 999.4516	4.493	4.456	3.833	−.037	−.623	1.019	.001
53 999.4599	4.513	4.469	3.859	−.044	−.609	1.013	.001
54 018.5163	4.502	4.468	3.841	−.034	−.627	1.064	.000
54 018.5223	4.491	4.462	3.842	−.029	−.619	1.074	.000
54 018.5298	4.498	4.465	3.844	−.033	−.621	1.088	.000
54 018.5374	4.502	4.464	3.840	−.038	−.624	1.104	−.001
54 018.5469	4.504	4.463	3.845	−.042	−.618	1.126	−.001
54 020.5750	4.492	4.456	3.842	−.036	−.614	1.226	−.002
54 020.5869	4.470	4.454	3.834	−.016	−.620	1.271	−.003
54 020.6016	4.506	4.468	3.845	−.038	−.623	1.335	−.004
54 106.2986	4.511	4.456	3.848	−.054	−.608	1.114	−.001
54 106.3069	4.514	4.458	3.850	−.055	−.608	1.134	−.001
54 106.3154	4.526	4.474	3.863	−.051	−.612	1.157	−.001
54 107.2210	4.466	4.434	3.828	−.032	−.606	1.012	.000
54 107.2284	4.467	4.431	3.814	−.036	−.617	1.016	.000
54 107.2355	4.478	4.445	3.829	−.033	−.616	1.022	.000
54 114.3142	4.508	4.460	3.837	−.048	−.623	1.224	−.002
54 114.3216	4.491	4.459	3.839	−.032	−.621	1.251	−.002
54 114.3290	4.503	4.461	3.851	−.041	−.610	1.280	−.003
54 116.2305	4.500	4.467	3.839	−.034	−.628	1.043	.000
54 116.2331	4.484	4.462	3.839	−.022	−.622	1.047	.000
54 116.2353	4.493	4.468	3.843	−.025	−.626	1.050	.000
54 120.2683	4.503	4.464	3.857	−.039	−.607	1.136	−.001
54 120.2712	4.510	4.486	3.876	−.024	−.610	1.143	−.001
54 120.2756	4.496	4.475	3.863	−.022	−.611	1.155	−.001
54 128.2456	4.485	4.465	3.845	−.020	−.621	1.135	−.001
54 128.2540	4.499	4.471	3.853	−.028	−.618	1.158	−.001
54 128.2623	4.495	4.460	3.846	−.035	−.614	1.182	−.001
54 128.2635	4.482	4.451	3.842	−.031	−.609	1.186	−.002
54 131.2606	4.500	4.466	3.846	−.034	−.620	1.203	−.002
54 131.2678	4.513	4.478	3.859	−.035	−.619	1.228	−.002
54 131.2706	4.519	4.488	3.871	−.031	−.617	1.238	−.002
54 132.2531	4.481	4.444	3.836	−.037	−.608	1.188	−.002
54 132.2601	4.480	4.445	3.837	−.035	−.608	1.211	−.002
54 132.2754	4.488	4.436	3.829	−.053	−.607	1.268	−.003
54 134.2449	4.504	4.460	3.842	−.044	−.618	1.180	−.001
54 134.2519	4.494	4.465	3.837	−.029	−.628	1.202	−.002
54 134.2587	4.493	4.459	3.847	−.034	−.613	1.226	−.002
54 296.5722	4.511	4.466	3.865	−.045	−.601	1.107	.000
54 296.5761	4.507	4.457	3.848	−.050	−.610	1.098	.000
54 308.5666	4.505	4.460	3.854	−.045	−.605	1.058	.001

Table B.5. continued.

Time of obs.	V	B	U	$B-V$	$U-B$	X	dX
54 308.5732	4.514	4.462	3.857	−.052	−.606	1.049	.001
54 308.5761	4.504	4.452	3.858	−.052	−.594	1.045	.001
54 320.5698	4.492	4.454	3.843	−.039	−.610	1.018	.001
54 320.5765	4.501	4.454	3.838	−.047	−.616	1.014	.001
54 320.5818	4.504	4.470	3.859	−.034	−.611	1.011	.001
54 356.4842	4.523	4.474	3.860	−.049	−.614	1.012	.001
54 356.4934	4.510	4.470	3.846	−.040	−.624	1.007	.001
54 356.5017	4.508	4.457	3.849	−.051	−.608	1.005	.001
54 464.2291	4.491	4.453	3.848	−.038	−.605	1.006	.001
54 464.2367	4.507	4.456	3.857	−.050	−.599	1.008	.001
54 464.2419	4.508	4.452	3.855	−.057	−.597	1.011	.000
54 468.2204	4.513	4.477	3.858	−.036	−.619	1.006	.001
54 468.2283	4.525	4.477	3.854	−.048	−.623	1.009	.000
54 468.2384	4.508	4.474	3.851	−.034	−.623	1.015	.000
54 474.2183	4.512	4.461	3.849	−.051	−.611	1.013	.000
54 474.2279	4.509	4.449	3.831	−.059	−.619	1.020	.000
54 474.2335	4.499	4.438	3.826	−.061	−.612	1.024	.000
54 492.2644	4.501	4.456	3.833	−.044	−.624	1.178	−.001
54 492.2699	4.501	4.459	3.840	−.042	−.619	1.195	−.002
54 492.2724	4.513	4.477	3.843	−.036	−.634	1.203	−.002
54 710.5267	4.509	4.460	3.858	−0.049	−0.602	1.006	0.001
54 710.5345	4.505	4.456	3.850	−0.049	−0.606	1.005	0.001
54 710.5412	4.505	4.456	3.857	−0.049	−0.599	1.004	0.001
54 719.5196	4.511	4.464	3.858	−0.047	−0.605	1.004	0.001
54 719.5276	4.506	4.456	3.858	−0.050	−0.598	1.005	0.001
54 719.5340	4.512	4.460	3.860	−0.052	−0.600	1.006	0.001
54 720.4839	4.496	4.446	3.839	−0.050	−0.608	1.014	0.001
54 720.4963	4.496	4.454	3.852	−0.041	−0.602	1.008	0.001
54 720.5030	4.490	4.448	3.850	−0.041	−0.598	1.006	0.001
54 754.3712	4.514	4.471	3.871	−0.042	−0.600	1.031	0.001
54 754.3773	4.509	4.469	3.869	−0.041	−0.600	1.025	0.001
54 754.3844	4.507	4.469	3.868	−0.038	−0.601	1.019	0.001
54 754.4082	4.509	4.466	3.860	−0.044	−0.606	1.006	0.001
54 754.4116	4.518	4.469	3.867	−0.048	−0.603	1.006	0.001
54 756.2655	4.521	4.479	3.881	−0.042	−0.598	1.269	0.001
54 756.2751	4.519	4.480	3.883	−0.039	−0.598	1.232	0.001
54 862.2424	4.504	4.458	3.844	−0.046	−0.614	1.153	0.001
54 862.2504	4.507	4.457	3.850	−0.050	−0.607	1.176	0.001
54 862.2571	4.519	4.456	3.842	−0.063	−0.614	1.196	0.002
55 062.5550	4.506	4.450	3.841	−0.057	−0.609	1.009	0.001
55 062.5643	4.507	4.448	3.844	−0.060	−0.603	1.006	0.001
55 062.5709	4.504	4.453	3.850	−0.051	−0.603	1.004	0.001
55 064.5333	4.505	4.448	3.854	−0.057	−0.594	1.019	0.001
55 064.5409	4.510	4.461	3.859	−0.050	−0.602	1.014	0.001
55 064.5473	4.525	4.469	3.872	−0.056	−0.598	1.010	0.001
55 065.5018	4.510	4.459	3.855	−0.052	−0.604	1.050	0.001
55 065.5110	4.513	4.452	3.844	−0.061	−0.607	1.038	0.001
55 065.5179	4.499	4.433	3.825	−0.067	−0.608	1.030	0.001
55 068.5090	4.519	4.464	3.866	−0.056	−0.598	1.031	0.001
55 068.5168	4.524	4.465	3.863	−0.060	−0.602	1.024	0.001
55 068.5229	4.522	4.460	3.867	−0.062	−0.593	1.019	0.001
55 070.5369	4.514	4.457	3.859	−0.057	−0.598	1.008	0.001
55 070.5463	4.503	4.442	3.844	−0.061	−0.598	1.005	0.001
55 070.5533	4.508	4.447	3.846	−0.061	−0.601	1.004	0.001
55 071.4694	4.515	4.455	3.862	−0.060	−0.594	1.076	0.000
55 071.4779	4.506	4.453	3.858	−0.053	−0.595	1.062	0.001
55 071.4841	4.514	4.458	3.856	−0.056	−0.602	1.052	0.001
55 072.5007	4.513	4.462	3.857	−0.052	−0.604	1.029	0.001
55 072.5083	4.517	4.462	3.860	−0.055	−0.602	1.022	0.001
55 072.5146	4.517	4.457	3.854	−0.061	−0.603	1.017	0.001
55 075.5818	4.516	4.461	3.866	−0.055	−0.595	1.019	0.000
55 075.5892	4.520	4.452	3.869	−0.068	−0.583	1.025	0.000
55 075.5952	4.520	4.461	3.863	−0.058	−0.598	1.031	0.000
55 076.3445	4.519	4.452	3.846	−0.067	−0.606	1.488	0.003

Table B.5. continued.

Time of obs.	V	B	U	$B-V$	$U-B$	X	dX
55 076.3486	4.520	4.455	3.852	−0.065	−0.603	1.462	0.003
55 076.3509	4.509	4.455	3.853	−0.054	−0.602	1.448	0.003
55 085.4286	4.522	4.473	3.864	−0.049	−0.609	1.082	0.000
55 085.4386	4.532	4.476	3.884	−0.056	−0.592	1.065	0.001
55 085.4473	4.509	4.453	3.854	−0.056	−0.599	1.052	0.001
55 098.5282	4.503	4.453	3.840	−0.050	−0.613	1.026	0.000
55 098.5373	4.509	4.454	3.848	−0.055	−0.605	1.035	0.000
55 098.5462	4.535	4.480	3.878	−0.055	−0.602	1.046	0.000
55 104.4275	4.517	4.454	3.853	−0.064	−0.601	1.018	0.001
55 104.4379	4.515	4.458	3.861	−0.056	−0.597	1.011	0.001
55 104.4457	4.510	4.443	3.842	−0.067	−0.602	1.008	0.001